Erlend Røneid

Pressure pulsations at Iveland Power Plant

Master's thesis in Mechanical Engineering

Supervisor: Bjørn Winther Solemslie

June 2020

Master's thesis

NTNU
Norwegian University of Science and Technology
Faculty of Engineering
Department of Energy and Process Engineering

NTNU
Norwegian University of
Science and Technology

Erlend Røneid

Pressure pulsations at Iveland Power Plant

Master's thesis in Mechanical Engineering
Supervisor: Bjørn Winther Solemslie
June 2020

Norwegian University of Science and Technology
Faculty of Engineering
Department of Energy and Process Engineering

NTNU
Norwegian University of
Science and Technology

NTNU
Norges teknisk-naturvitenskapelige universitet
Institutt for energi- og prosessteknikk

EPT-M-2020

MASTEROPPGAVE

for

Student Erlend Røneid

Våren 2020

Trykkpulsasjoner ved Iveland Kraftverk
Pressure pulsations at Iveland Power Plant

Bakgrunn
Agder Energi har erfart mye støy ved Iveland II Kraftverk som ligger i Otra ca. 27 kilometer nord for Kristiansand, mellom Byglandsfjorden og Otras utløp. Dette er støy som oppstår på dellast og forsvinner helt når effekten passerer 28 MW. Det kan tyde på at årsaken kommer fra strømningen i sugerøret. Turbinen er utstyrt med luft innslipp gjennom turbinaksling til sugerøret og dette prosjektet kan forsøke med forskjellige luftmengder for å redusere støy. Det er ønskelig å gjennomføre trykkpulsasjon-måling på turbinen for å se om man kan finne årsaken til støy problemet.

Mål
Gjennomføre trykkpulsasjon-målinger ved Iveland Kraftverk

Oppgaven bearbeides ut fra følgende punkter:

1. Litteraturstudie
    a. Evaluering av trykkpulsasjoner i Francis turbiner
2. Software
    a. Labview skal benyttes for målinger
    b. Matlab skal benyttes til evaluering av resultater
3. Forberedelser i Vannkraftlaboratoriet
    a. Gjennomføre statisk og dynamisk amplitudekalibrering av instrumenter som skal benyttes til trykk-måling på kraftverket
4. Måling på Iveland Kraftverk
    a. Gjennomføre trykkmåling er på hele operasjonsområdet
    b. Om mulig gjennomføre trykkmålinger ved utvalgte driftspunkt med en annen mengde luftinnslipp
    c. Evaluering av måleresultater
    d. Utarbeide apparat for dynamisk kalibrering av trykksensorer med frekvensstyring ved Vannkraftlaboratoriet
5. Dersom studenten skal dra til Nepal på ekskursjon så skal tidligere arbeid fra prosjektet og det videre arbeidet i denne hovedoppgaven bli skrevet som en egen publikasjon og presentert på konferansen: 10th International symposium on Current Research in Hydraulic Turbines (CRHT-X) ved Kathmandu University 31. mars 2020.
6. Dersom det er tid tilgjengelig:
    a. Ferdigstille det utarbeidede apparatet for dynamisk kalibrering
    b. Gjennomføre kalibrering av sensorer brukt ved Iveland for å validere resultatene

Abstract

The energy market is transitioning to more renewable energy sources. Hydropower, known for its high efficiency, reliability and superior regulating abilities compared to other renewable energy sources, has an important role in this transition. The use of hydropower for regulating the power demand increases the power plants part load operation.

Iveland II is a hydro power plant located in Aust-Agder in Norway hosted by Agder Energi. The plant is experiencing a lot of vibrations and noise when it is operating at part load, limiting the operating range for the turbine. Agder Energi has asked the Waterpower laboratory at NTNU for help to find the source of the noise and vibrations.

In order to to investigate the source of the noise and vibrations, pressure measurements were conducted at the power plants draft tube and inlet. Pressure measurements were performed with varying air flow through the shaft and in to the draft tube to investigate how this affected the pressure pulsations.

The FFT analysis showed that the Rheingans frequency is dominant both at the inlet and in the draft tube when operating at part load. Its low frequency of $\sim$ 1 Hz ruled it out as a possible noise source. Based on simple calculations possible frequencies caused by Von Kármán vortices were found to be in the range of the frequencies observed. The investigation of a gas bubble acting as a free water surface in the draft tube revealed it as a potential source. The measurements conducted in this thesis are not enough to conclude.

Restricting the air flow entering the draft tube through the turbine shaft proved to have little effect on the pressure pulsations.

A dynamic calibration device was designed but was not manufactured.

Samandrag

Energimarkedet går over til meir fornybare energikjelder. Vasskraft, kjent for sin høge effektivitet, pålitelegheit og overlegne reguleringsemne samanlikna med andre fornybare energikjelder, har ein viktig rolle i denne overgangen. Bruken av vasskraft for å regulera kraftbehovet aukar kraftverkets drift i dellast området.

Iveland II er et vasskraftverk lokalisert i Aust-Agder i Norge som er drifta av Agder Energi. Anlegget opplever mykje vibrasjonar og støy når det opererar på dellast, og det begrensar driftsområdet for turbinen. Agder Energi har bedt Vasskraftlaboratoriet ved NTNU om hjelp til å finne kjelda til støyen og vibrasjonane.

For å undersøke kjelda til støyen og vibrasjonane blei det utført trykkmålingar ved kraftverkets sugerøyr og innløp. Trykkmålingar blei og utført med varierande luftinnslipp, som går gjennom turbinakslingen og inn i sugerøyret, for å undersøka korleis dette påverka trykkpulsasjonane.

FFT-analysen viste at Rheingans frekvensen er dominerande både ved innløpet og i sugerøyret når turbinen opererer på dellast. Dens låge frekvensen på $\sim$ 1 Hz utelukka den som ein mogeleg støykjelde. Basert på enkle berekningar blei det funnet at frekvensar forårsaka av Von Kármán virvlar ligg i området for observerte frekvensar. Undersøkinga av en gassboble som fungerer som eit fritt vasspeil i sugerøyret viste at det kan vere ein potensiell kjelde. Målingane gjort i denne oppgåva er ikkje nok til å konkludera.

Begrensing av luftstraumen som blir slept inn i sugerøyret gjennom turbinakslingen viste seg å ha liten innverknad på trykkpulsasjonane.

Ein dynamisk kalibreringsenhet ble designa, men blei ikkje produsert.

Preface

This master thesis was written at the Waterpower laboratory at NTNU in the spring of 2020 as a continuation of the specialisation project conducted in the fall 2019. The main part of the objective in this thesis is provided by Agder Energi, which is an energy company based in Kristiansand, Norway.

I would like to thank my supervisor Bjørn Winther Solemslie for the guidance and support during this project. I would also like to thank my co-supervisors Ole Gunnar Dahlhaug and Johannes Opedal Kverno for their help in analysing the data. Also thanks to Bård Aslak Brandåstrø, who traveled to Iveland with me and provided support during the pressure measurements, and Halvor Haukvik who helped me design the dynamic calibrator.

In addition, I would like to thank Inge Lines at Agder Energi for providing a interesting task. I would also like to thank Per Olav Engen who made sure the measurements at Iveland went well.

Erlend Røneid
Odda, June 28 2020

Contents

Objective **i**

Abstract **iii**

Samandrag **v**

Preface **vii**

Contents **xii**

List of Tables **xiii**

List of Figures **xv**

List of Symbols **xix**

1 Introduction **1**

1.1 Background 1

1.2 Scope 2

2 Theory **5**

2.1 The Francis turbine 5
2.2 Pressure pulsations 6
2.2.1 Rotor Stator Interactions 6
2.2.2 Von Kármán Vortex 7
2.2.3 Draft Tube Vortex 8
2.2.4 Pressure waves in the waterway 11
2.3 Frequency Analysis 12
2.3.1 Sampling Frequency 12
2.3.2 DFT analysis 13
2.4 Dynamic calibration 14
2.4.1 Previous work 15
2.5 Uncertainty in measurements 16

3 Methodology **19**
3.1 Health, Safety and Environment 19
3.2 Performing measurements at Iveland II 19
3.2.1 Air intake 22
3.2.2 Sound recording 23
3.2.3 Data acquisition and processing 24
3.3 Uncertainty calculations 25

4 Results **27**
4.1 Pressure pulsations 27
4.1.1 General information 27
4.1.2 Observations during the measurements 27
4.1.3 Time series and peak to peak 28

4.1.4 FFT analysis 30
4.1.5 Spectrogram of audio 34
4.1.6 Von Kármán vortex and pressure waves in the water way . 35
4.1.7 Synchronous and Asynchronous component 38
4.1.8 Air injection 41
4.2 Dynamic calibrator 43

5 Discussion **47**
5.1 General observations 47
5.2 FFT analysis 47
5.3 Spectrogram of audio 48
5.4 Von Kármán vortices and pressure waves in the waterway 49
5.5 Synchronous and Asynchronous component 49
5.6 Air injection 50
5.7 Dynamic Calibrator 50

6 Conclusion **53**

7 Further work **55**

References **57**

Appendix **A1**

A Health, Safety and Environment **A1**
A.1 Job Safety Analysis A1
A.2 Communication plan A5

B Drawings of Dynamic calibrator **B1**

C CRHT-X Paper **C1**

D Calibration reports **D1**

E Documentation for pressure sensors **E1**

List of Tables

1.1 General information about Iveland II [1] 2

3.1 Measurement points 21
3.2 List of equipment 24
3.3 Maximum uncertainty from the calibration 26

4.1 Known frequencies 27
4.2 Dominating frequencies at Inlet sensor 31
4.3 Dominating frequencies at Draft tube sensor 1 32
4.4 Dominating frequencies at Draft tube sensor 2 33
4.5 Air velocity at different operating points 41
4.6 List of components for the dynamic pressure generator 45

List of Figures

1.1 Map showing the location of Iveland II in Aust-Agder [2] 2

2.1 Section view of a turbine showing the main components [3] 5

2.2 Damage caused by RSI [4] 7

2.3 **a)** shows the velocity triangle with the guide vanes at BEP, **b)** shows guide vanes below BEP and **c)** show the guide vanes above BEP 8

2.4 Vortex rope. Photo: Bjørn Winther Solemslie 9

2.5 Damage caused by Vortex rope [4] 10

2.6 Examples of passive methods to reduce pressure pulsations caused by the draft tube vortex [5] 11

2.7 Aliasing with sampling frequency of 1.5 the actual signal. Figure Johannes Opedal Kverno [6] 12

2.8 A sampled signal of a measurement done in the Waterpower laboratory 13

2.9 Different stages of welch method 14

2.10 The set up for dynamic calibration [3] 16

3.1 Placement of pressure sensors on the draft tube 20

3.2 Draft tube pressure sensor 2, with the transition piece 21

3.3 Inlet pressure sensor 22

3.4 The device used for measuring the air velocity [7]. 23

3.5 Air intake in the drain room 24

3.6 Hole drilled for measuring air velocity 24

3.7 Low range dead weight tester 26

4.1 Time series from the inlet sensor. 28

4.2 Time series from Draft tube 1. 29

4.3 Time series from Draft tube 2. 29

4.4 Peak to peak values for all measuring points with confidence interval of 97 %. Uncertainty band is multiplied with 100. 30

4.5 FFT for the inlet sensor. The frequency is normalized with the rotational frequency. The amplitude is normalized with the design head. 31

4.6 FFT for the Draft tube 1 sensor. The frequency is normalized with the rotational frequency. The amplitude is normalized with the design head. 32

4.7 FFT for the Draft tube 2 sensor. The frequency is normalized with the rotational frequency. The amplitude is normalized with the design head. 33

4.8 The mean pressure value for all operating points in the draft tube. the uncertainty is multiplied by 10. 34

4.9 Spectrogram of sound recording 27 MW to 23 MW 35

4.10 Von Kármán frequency at different trailing edge lengths and flow velocity 36

4.11 Pulsation frequency with different lengths between water surfaces and speed of sound in the water way 37

4.12 Pulsation frequency with different lengths between water surfaces and speed of sound in the water way and harmonic number $j = 2$. 37

4.13 Synchronous and Asynchronous component at 43 MW 38

4.14 Synchronous and Asynchronous component at 27 MW 39
4.15 Synchronous and Asynchronous component at 23 MW 39
4.16 Synchronous and Asynchronous component at 19 MW 40
4.17 Synchronous and Asynchronous component at 15 MW 40
4.18 FFT at 23 MW of Draft tube sensor 1 with restricted air flow . . . 42
4.19 Mean values at 23 MW with restricted air flow 42
4.20 Peak to peak values at 23 MW with restricted air flow. Uncertainty is multiplied by 10 43
4.21 The dynamic calibrator with all its components mounted 44
4.22 Half section view of the main body showing all inlets 46
4.23 Half section view of the main body showing the valves 46

List of Symbols

Latin Symbols

A	Area	m^2
a	Speed of sound in water	m/s
c	Actual velocity	m/s
c_m	Radial component of actual velocity	m/s
c_u	Tangential component of the actual velocity	m/s
e_{tcal}	Total calibration error	$-$
e_{rcal}	Random error in calibration	$-$
e_{rmes}	Random error in measurement	$-$
e_{scal}	Systematic error in calibration	$-$
e_{smes}	Systematic error in measurement	$-$
e_{totl}	Total error	$-$
f	Frequency	Hz
f_e	Expected frequency	Hz
f_g	Guide vane frequency	Hz
f_n	Rotational frequency	Hz
f_p	Rheingans frequency	Hz

f_r	Blade passing frequency	Hz
f_{res}	Frequency resolution	Hz
f_s	Sampling frequency	Hz
f_t	Waterway frequency	Hz
f_v	Von Kármán frequency	Hz
f_{grid}	Grid frequency	Hz
H_0	Design head	m
j	Harmonic number	$-$
L	Characteristic length	cm
L_t	Length to nearest free water surface	m
N	FFT size	$-$
n	Number of samples	$-$
p_{async}	Asynchronous pressure component	kPa
p_{sync}	Synchronous pressure component	kPa
Q	Volume flow rate	m^3/s
s	Standard deviation	$-$
St	Strouhal number	$-$
$t_{\alpha/2}$	Student t value	$-$
u	Circumferential velocity	m/s
v	Velocity component of main flow	m/s
v_{avg}	Average velocity	m/s
v	Relative velocity	m/s
x_i	Measured value	$-$
$\overline{x}$	Mean value	$-$
Z_g	Number of guide vanes	$-$

Z_r	Number of runner blades	–

Greek Symbols

α	Confidence interval	%
β	Angle of relative velocity	°

Abbreviation

BEP	Best efficiency point
DT1	Draft tube sensor 1
DT2	Draft tube sensor 2
DFT	Discrete Fourier transform
FFT	Fast Fourier transform
RPM	Rotations per minute
RSI	Rotor stator interactions
RSS	Root square sum

Chapter I

Introduction

1.1 Background

The energy market is transitioning to more renewable energy sources. Hydropower, which is known for its high efficiency, reliability, and superior regulating abilities compared to other renewable energy sources, has an important role in this transition [8]. The use of hydropower for regulating the power demand increases the part load operation of power plants [9]. Operating a turbine outside its design point can cause problems such as pressure pulsations and reduced life expectancy.

Iveland II is a hydro power plant located in Aust-agder in Norway hosted by Agder Energi. It lies next to the river Otra and exploits a height difference of 50 m between Gåseflåfjorden and Skaiåevja. The plant is experiencing a lot of vibrations and noise when it is operating at part load, limiting the operating range for the turbine. Agder Energi has asked the Waterpower laboratory at NTNU for help in finding the source of the noise and vibrations.

A common way of investigating this issue is to perform pressure measurements. The sensor used for this purpose is often calibrated using a static calibration method. A static calibration does not represent its dynamical behaviour and therefor it is desirable to perform a dynamical calibration. This will increase the accuracy with respect to the frequency and amplitude of the measurements. When conducting field measurements the pressure sensors are ideally flush mounted with the wall. This is often not possible and the water way between the sensor and the pressure source will affect the result. With a dynamic calibrator it is possible to investigate how the measurements are affected by this.

Figure 1.1: Map showing the location of Iveland II in Aust-Agder [2]

Table 1.1: General information about Iveland II [1]

Iveland 2 power plant	
Design head	50m
Turbine	Francis
Rated power	44 MW
BEP	$\sim$ 39 MW
Commissioned	2016
RPM	176,47

1.2 Scope

To investigate the source of the noise and vibrations, pressure measurements were conducted at the power plants draft tube and inlet. The results where processed in MATLAB and analysed in the search for the source of the vibrations. The power plant has installed an air intake through the shaft and into the draft tube. Pressure measurements were performed with varying air flow to investigate how this affected the pressure pulsations.

Further a device for dynamic calibration of pressure sensors was designed. This

design was based on an idea of Halvor Haukvik and Einar Agnalt who made a similar device that did not function as intended. The apparatus they used for shifting the valve position had to abrupt movements causing disturbances in the measured signal and prevented a sufficient calibration measurement.

Chapter II

Theory

2.1 The Francis turbine

The Francis turbine was named after James B. Francis who in 1849 proposed the concept of radial in flow and axial out flow in a hydraulic turbine [10]. In a Francis turbine the water enters the spiral casing and gets distributed throughout the circumference. The stay vanes provide structural support to the spiral casing and designed to minimise the disturbance in the flow. The guide vanes regulate the power output and guides the flow in the optimal direction towards the runner blades. The runner blades guide the water through the runner changing its direction from radial to axial causing the runner to rotate. The runner extracts both potential and kinetic energy by reducing the pressure and changing the direction of the flow. The draft tube connects the runner exit with the tail race [10].

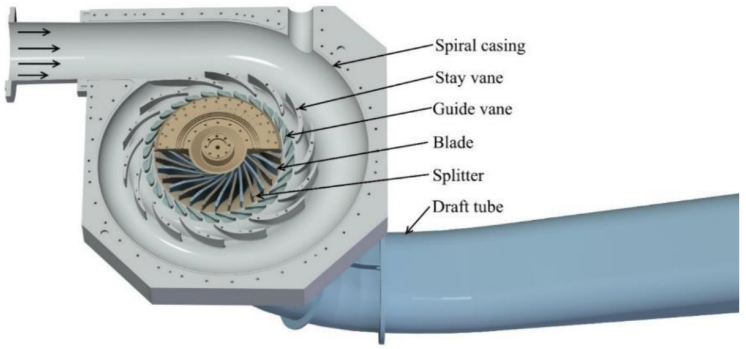

Figure 2.1: Section view of a turbine showing the main components [3]

2.2 Pressure pulsations

The theory section concerning Pressure pulsations is taken from the specialisation project "Pressure pulsations at Iveland Power Plant", written by the author [11], with some minor changes.

2.2.1 Rotor Stator Interactions

The runner blades have a low-pressure and high-pressure side. This pressure field moves with the runner blades, and will create a pressure pulsation each time a blade passes the guide vane [4]. The frequency of the pressure pulsation is therefore connected to the number of blades. The pulsation will move from the vaneless space and through the guide vanes and into the spiral casing [12]. This is called the blade passing frequency and can be calculated with the following equation.

$$f_r = f_n \cdot Z_r \cdot j \tag{2.1}$$

Where f_n denotes the rotational speed in revolutions per second, Z_r denotes the number of blades and j denotes the harmonic number.

The runner channels will also experience a non-uniform pressure and velocity field coming from the guide vanes. This will create a pressure pulsation each time a guide vane passes the blade. The frequency of the pressure pulsation is therefor connected to the number of guide vanes. This pulsation will move through the runner. The guide vane frequency can be calculated with the equation below.

$$f_g = f_n \cdot Z_g \cdot j \tag{2.2}$$

Where Z_g is the number of guide vanes.

The amplitude will be highest when the guide vanes are close to the runner and will decrease as they move away [4]. Therefor it may be expected a higher amplitude at high guide vane opening versus low guide vane openings.

Effects There is a risk of high dynamic stress in Francis turbines caused by Rotor Stator Interactions (RSI). This can happen in the presence of a high amplitude RSI with a frequency close to the natural frequency of the runner. The natural frequency of an object is the frequency it oscillates with when it is set to vibrate and then left with no driving or dampening source [13]. If an object is affected by a periodic force that is close to its natural frequency it will start to oscillate with the same frequency and a relatively high amplitude. This phenomenon is called resonance. Examples of this has led to runner failure within hours of operation [4]. Other examples of damages caused by RSI is shown in Figure 2.2. The left picture shows a crack starting at the runner blade close to the hub.

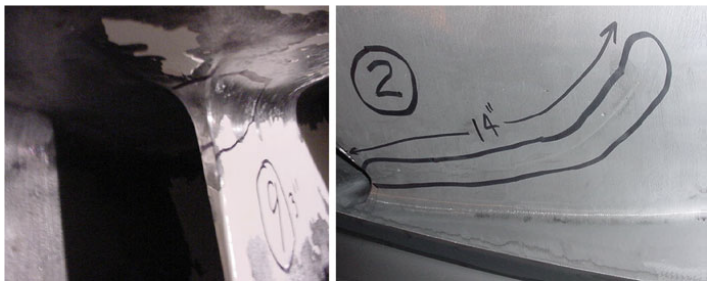

Figure 2.2: Damage caused by RSI [4]

Countermeasures Measures to avoiding resonance vibrations in the runner is mainly taken in the design phase. The number of guide vanes and runner blades must be selected so they do not create unwanted vibrations, pulsations, and noise. For an already installed runner, the options are limited. Reinforcements can be mounted, increasing the stiffness and changing the natural frequency. This is often a temporary solution due to the flow obstruction. Changing the runner with a newly designed one is an option [4].

2.2.2 Von Kármán Vortex

Von Kármán vortices are formed in the wake downstream of a bluff body placed in perpendicular flow [4]. The separation point behind the body will alternate between the two sides, creating alternating swirls in the wake. The frequency of the vortex shedding can be calculated using the equation below [4].

$$f_v = \frac{St \cdot v}{L} \tag{2.3}$$

Where L denotes a characteristic lateral dimension of the body, v denotes the velocity component of the main flow relative to the body. St denotes the Strouhal number which depend on the shape of the body and the Reynolds number. The Strouhal number lies in the range of 0.18-0.22 for a large range of Reynolds numbers [14]. For a turbine blade the characteristic length L would be the thickness of the trailing edge.

Effects If the frequency of the vortex shedding coincides with the natural frequency of the body creating them, it will lead to resonant vibration. This might cause fatigue resulting in cracks in important components. In large hydraulic machinery this can happen in the stay vanes, guide vanes and at the runner blades

[4].

Countermeasures For avoiding resonance from the pressure pulsations caused by Von Kármán vortices, the main effort is done in the design phase. The stay vanes, guide vanes and runner blades must be design so the trailing edge only produce low-intensity vertices. If resonance happens to occur anyway, it is possible to add the stiffness to the structure. That may also change the natural frequency, thus, prevent resonance [4].

2.2.3 Draft Tube Vortex

At operational points differing from the design conditions, the water leaving the runner blade will have a velocity component that moves in the tangential direction, as shown in Figure 2.3. This creates a swirl in the draft tube because the angle β and rotational speed u is fixed, and the flow rate is off the design point. Experiments have shown that swirling flow in a pipe tend to separate the flow in to two regions, where the volume flow driving movement of water mainly happens at the outer region [4]. When the swirl ratio becomes big enough, a stagnation point forms in the inner region.

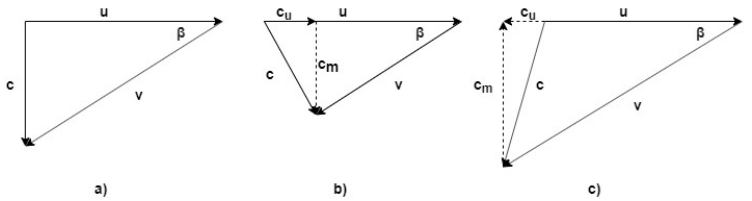

Figure 2.3: a) shows the velocity triangle with the guide vanes at BEP, **b)** shows guide vanes below BEP and **c)** show the guide vanes above BEP

At part load, a helix shaped vortex might appear at the border between the two regions, often referred to as a 'Rotating Vortex Rope'. If the pressure in the draft tube becomes lower than the vapour pressure, the vortex rope becomes visible due to cavitation, as shown in Figure 2.4. This rope creates a pressure pulsation as it is rotating in the draft tube. The frequency of the pulsation is called the Rheingans frequency, named after W.J. Rheingans [4], who estimated the relative frequency to behave like the equation below.

$$\frac{f_p}{f_n} \simeq 0.278 \tag{2.4}$$

Where f_p is the frequency of the pressure pulsation created by the vortex rope and

f_n is the runner frequency. The vortex rope pulsation consists of two components with the same frequency, an asynchronous and a synchronous component [5]. The synchronous part has equal phase and amplitude in cross section and may be seen as an axisymmetric pressure wave as it propagates through the draft tube. The asynchronous part has a pressure pattern moving around the axis of the draft tube. The components can be calculated using the following equations [5].

$$p_{sync} = \frac{DT1 + DT2}{2} \tag{2.5}$$

$$p_{async} = \frac{DT1 - DT2}{2} \tag{2.6}$$

Where $DT1$ and $DT2$ are pressure signals from the same plane but placed 180 degrees apart from each other.

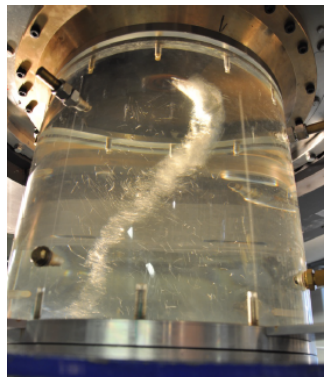

Figure 2.4: Vortex rope. Photo: Bjørn Winther Solemslie

Effects The draft tube vortex may not a significant effect on the runner itself but operating for long periods with vortex rope conditions may have destructive effects on draft tube component such as the cone, door, and surrounding concrete. An example of this is shown in Figure 2.5, where the concrete has cracked by the draft tube door. Both RSI and vortex rope can excite vibrations in the penstock. Exposed penstocks, i.e. penstocks that are not fully surrounded by rock or earth, are especially sensitive to vibrations and may reach levels that are not acceptable.

Countermeasures Different methods are available to mitigate pressure pulsations caused by a draft tube vortex. They can be divided in to active and passive methods [5]. Examples of active methods are air and water injection, while passive methods might be fins and shaft extension.

Figure 2.5: Damage caused by Vortex rope [4]

Air injection can dampen the high frequency components of the vibration and noise. Common methods of injecting air into the draft tube is through the shaft, and peripheral injection through the draft tube wall. Water may also be used as a working fluid to prevent pressure pulsations. Experiments have been performed where nozzles are mounted at the draft tube wall, angled towards the swirl [5]. The result is that the amplitude of the pressure pulsations is reduced. It can also have a positive effect when the turbine is operating above BEP even though the nozzles then become angled in the direction of the swirl [15]. Another way of injecting water is in the axial direction at the draft tube centre. The water that is injected can be taken from the penstock, but as it is bypassing the turbine it will be counted as a loss. All these methods will affect the efficiency of the turbine in some degree but might prolong the life of the mechanical equipment.

Examples of passive methods can be seen in Figure 2.6. Figure 2.6(a) show a draft tube where fins have been mounted. Installing fins has proven to reduce the draft tube swirl and the amplitude of the pressure pulsations. Another alternative is to mount an extension on the runner cone shown inn Figure 2.6(a). Experiments have shown that a runner cone will reduce the amplitude by moving the starting point of the vortex rope downstream [5]. The rope will then have a shorter distance to develop.

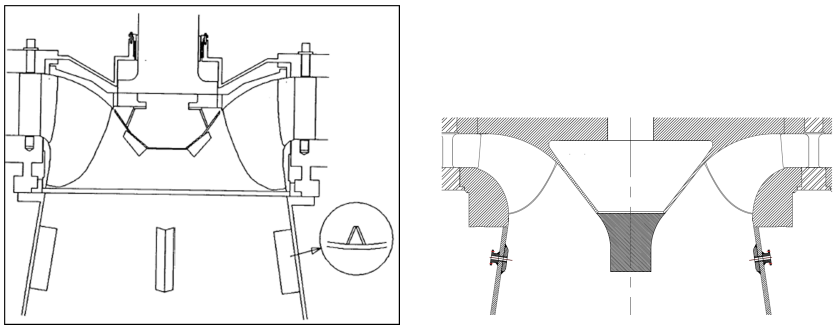

(a) (b)

Figure 2.6: Examples of passive methods to reduce pressure pulsations caused by the draft tube vortex [5]

2.2.4 Pressure waves in the waterway

Changing the volume flow in the waterway will cause pressure waves [16]. If a valve is closed rapidly it will stop the water cause the pressure to rise in front of the valve and a pressure wave will move up the pipe. Once all the water in the pipe has stopped the high pressure will push the water in the direction of the reservoir, resulting in a low pressure in the tunnel. This will cause the water to flow back towards the valve. This phenomenon is often referred to as water hammer. The frequency of the pressure wave travelling up and down between the nearest free water surface and the valve are given by the equation seen below.

$$f_t = \frac{j \cdot a}{4 \cdot L_t} \tag{2.7}$$

Where a denotes the speed of sound in the water way, j denotes the harmonic number and L_t denotes the length to the nearest free water surface. Closed valves will have odd harmonic, $j = 1, 3, 5...$ [17]. The speed of sound in water way depends on its air content and the stiffness of the walls. If the valve is not completely closed when the pressure pulse to return, the frequency will behave more like Equation 2.8.

$$f_t = \frac{j \cdot a}{2 \cdot L_t} \tag{2.8}$$

Open valves will have even harmonics, $j = 2, 4, 6...$ [17]. The equation also applies

if the pressure pulse is moving between to free surfaces. In this case the pressure at each end is determined by the ambient pressure and therefore the characteristic is not the same as in equation 2.7 [6].

2.3 Frequency Analysis

2.3.1 Sampling Frequency

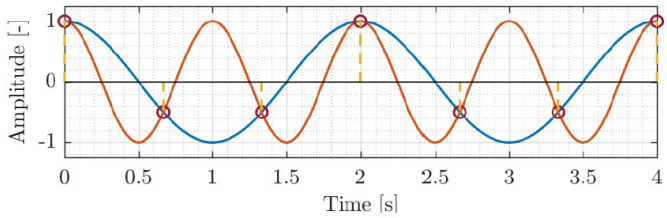

Figure 2.7: Aliasing with sampling frequency of 1.5 the actual signal. Figure Johannes Opedal Kverno [6]

When a continuous physical signal is recorded, the signal is sampled and stored as a series of discrete digital values. The rate that these values are sampled at is important in order to achieve a good measuring result. If the sampling frequency is to low, aliasing may occur. Aliasing is when the physical signal can be interpreted as different signal with other properties. Figure 2.7 shows how aliasing can occur when the sampling frequency is 1.5 times the physical signal. Nyquist sampling theorem states the following [18].

$$f_s \geq 2 \cdot f_e \tag{2.9}$$

Where f_s denotes the sampling frequency and f_e denotes the expected frequency of the signal. This indicates that in order to avoid aliasing, the sampling rate needs to be at least two times the size of the highest expected frequency in the signal.

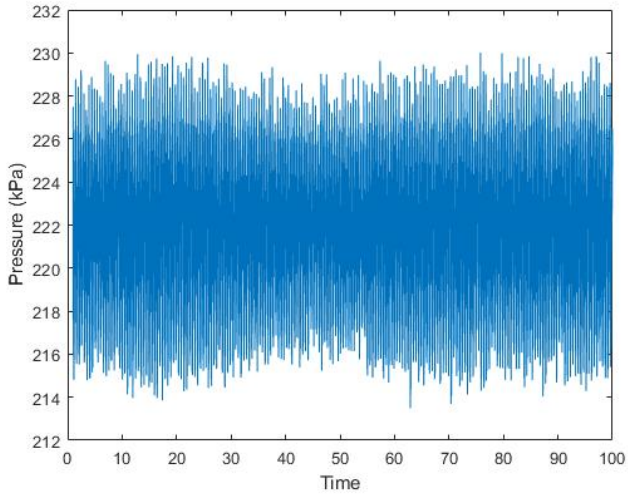

Figure 2.8: A sampled signal of a measurement done in the Waterpower laboratory

2.3.2 DFT analysis

Figure 2.8 show sampled values that are plotted in the time domain. It is difficult to read any results from that. In order to analyse the result, it is useful to transform the signal to the frequency domain. The transformation is done by using a Discrete Fourier transform (DFT). One version of DFT that is commonly used is Fast Fourier Transform (FFT) [19]. When the FFT is performed several frequency bins are created [20]. These bins present the energy that the signal has at this frequency. The frequency resolution is the width of between each bin and therefor dictates the accuracy of the result. Frequency resolution is calculated with the equation below.

$$f_{res} = \frac{f_s}{N} \tag{2.10}$$

Where f_s denotes the sampling frequency and N denotes the size of the FFT.

Windowing

The DFT assumes that the signal is periodic, but if the frequency of the signal is not an exact multiple of the frequency resolution, the DFT will see a discontinuity between the last and the first sample. This will spread the power out on the whole spectrum. To avoid this, the signal is multiplied with a 'window function' before the

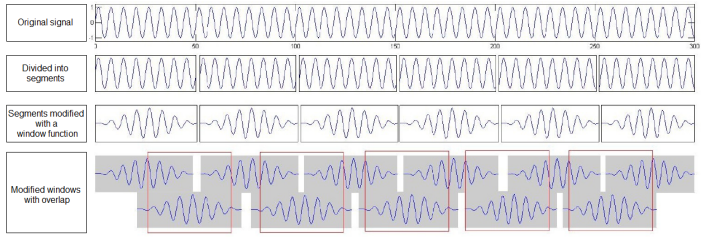

Figure 2.9: Different stages of welch method

DFT is performed. One example of this is the Hanning window. The function starts near zero and increases towards the middle of the segment, before it decreases back to near zero, as illustrated in line three in Figure 2.9. In that way the discontinuity is removed.

Welch's method

The signal from the sensor will contain some noise. To deal with this the signal is divided into sections, before the window function is applied, illustrated in line two in Figure 2.9. The power of each frequency is calculated for the individual sections and then an average is calculated for all sections. One drawback doing this is that the frequency resolution is decreased.

Since the window function gives values close to zero at the edges of each section, a significant part of the data will not contribute effectively to the analysis. A solution to get maximum information out of the recorded data, is to have the sections overlap, as line four in Figure 2.9 illustrates. By how much depends on which window function that is used. The sectioning and overlap together with the windowing is often referred to as the Welch method.

2.4 Dynamic calibration

When pressure pulsations are measured the accuracy is dependent on the measuring equipment. It is therefore necessary to know the uncertainty of the pressure transducer in a dynamic environment. Most pressure sensors are only calibrated by static calibration methods, as no standardized method for dynamic secondary calibration or a primary calibration method for reference is available [21].

Dynamic calibration of pressure sensors depends on a dynamic pressure generator that produces a measurand with a known behaviour [22]. In some cases, the generated pressure can be predicted accurately regarding frequency and amplitude. If

not, a reference pressure sensor is necessary to predict the generated pressure.

Dynamic pressure generators can be classified as either periodic or aperiodic [22]. The aperiodic can be characterised by the pulse shape they produce in form of a quick pressure step or a peaking pulse. Examples of aperiodic generators are shock tube and shockless step generators. A shock tube consists of two tubes separated by a thin diaphragm. The two tubes are pressurised with different pressure levels causing the diaphragm to burst. This will make a shock wave to travel in the low pressure tube. Behind this shock wave the pressure will be higher causing a positive pressure step that is registered by the calibration sensor and reference sensor [22]. Shockless pressure-step uses a quick acting valve to create a pressure step between to pressure levels. The device is designed in a way that it prevents a shock wave from forming. The advantage with this device is its wide pressure ranges in both the initial value and the step.

A periodic pressure generator would ideally produce known pressure inputs and frequency for the calibrating sensor. If the average pressure and dynamic amplitude is not known a reference sensor must be used. The pressure generator produces a pressure pulse in a chamber were both the calibrator and reference sensor are connected. The sensors must be mounted close, so they experience the same pressure. That includes amplitude, shape, and phase lag [22]. The pressure pulse is created by either varying the volume or mass in the chamber. For varying the volume, a piston or a diaphragm may be used. The varying mass uses a fast-acting valve to control the in and out flow of the chamber. For both generators it is important that the chamber is sufficiently small, so the natural frequency is far away from the frequency imposed.

2.4.1 Previous work

As a part of his doctoral thesis work Einar Agnalt made a device for dynamic calibration together with Halvor Haukvik. This device is a periodic pressure generator with fixed volume and varying mass. This is done with fast acting valves to alter between low and high pressure. The high and low pressure was created with two dead weight calibrators with different pressure ranges, in order to establish known pressure sources. The setup is illustrated in Figure 2.10.

When testing the device, it was discovered that the device managing the valves caused disturbance in the signal when it was operating. Therefor the device was unsuited as a periodic generator. Instead Einar Agnalt used it as an aperiodic generator by creating a pressure step in order to check the repeatability. This was done by letting the pressure alternate between 100 kPa and 90 kPa with a frequency of 1 Hz [3].

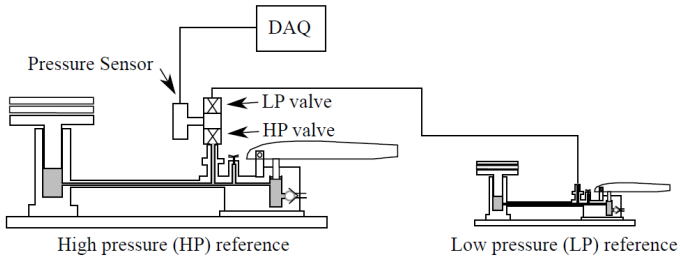

Figure 2.10: The set up for dynamic calibration [3]

2.5 Uncertainty in measurements

When measurements are performed, they always include some level of uncertainty. As the source of these inaccuracies IEC 60193 [23] considers three errors:

- Spurious error
- Random error
- Systematic error

Spurious errors are caused by human error or malfunction in the instrument. These errors should not be included, and the corresponding measurement shall be removed.

Random error is caused by various small, independent influences that cause the measurement system to show different readings when the same input is given. The distribution in the measurements usually approaches a normal distribution when the number of measurements is increased. To compensate for a small sampling size in the assumption of normal distribution, the Student-t confidence interval is used. The random error is found using Equation 2.11.

$$e_{rcal} = \pm \frac{t_{\alpha/2} \cdot s}{\sqrt{n}} \tag{2.11}$$

where n denotes the number of measurements, $t_{\alpha/2}$ denotes the student t value and s denotes the standard deviation. The student's t value depends on the confidence interval α chosen, and n. The standard deviation is given by the equation below.

$$s = \left(\frac{\sum_{i=1}^{n} (x_i - \overline{x})}{n-1} \right)^{1/2} \tag{2.12}$$

where x_i denotes the measured value and $\overline{x}$ denotes the mean value for all the measured values. Both of these equations gives a smaller value as n gets bigger. In other words more measurements reduces the error.

Systematic error may be linked to poorly calibrated instruments, hysteresis or lack of linearity in the instrument [24]. This error cannot be reduced by increasing the number of measurements. To obtain the magnitude of error one must evaluate the calibration procedure including the calibration method and random errors during the calibration.

The total uncertainty of the calibration is calculated by combining the systematic, e_{scal} and random error e_{rcal} in the Root Square Sum (RSS) method given in the following equation.

$$e_{tcal} = \sqrt{(e_{scal})^2 + (e_{rcal})^2} \tag{2.13}$$

For the total uncertainty in the calibration e_{tcal} becomes a systematic error in the measurement. Systematic error e_{smes} and random error e_{rmes} in the measurement are used in the RSS method again to calculate the total uncertainty e_{tot}.

$$e_{tot} = \sqrt{(e_{smes})^2 + (e_{rmes})^2} \tag{2.14}$$

Chapter III

Methodology

3.1 Health, Safety and Environment

According to the guidelines of the institute there has been performed a risk assessment of the field work. The risk assessment, along with communication plan for the trip, can be found in Appendix A

3.2 Performing measurements at Iveland II

As a part of the preparations for the measurements an inspection of the power plant was done in November 2019 in order to get an understanding of what the issue at Iveland II was. To do so the plant was operated at different points in the range of 44 MW to 10 MW.

In addition to inspect the problem area, the location of the pressure sensor was to be decided. The draft tube at Iveland II has four outtakes placed 90 degrees apart. It was decided to use two of them placed opposite of each other shown in Figure 3.1. That way it is possible to find the synchronous and asynchronous pressure component of the Vortex rope pulsation. To be able to connect the pressure sensors without stopping the power plant, Agder Energi mounted vales between the outtake and the pipe. The placement also allowed the pressure sensors to be placed close to the pressure source, avoiding the dampening effect of a pipe or hose. For the pressure sensor at the inlet several options were considered but the choice fell on a valve mounted on manhole hatch shown in Figure 3.3. This allowed quick access and a short distance from the pressure source. Between the sensors and the valve there was a transition piece. This piece, seen in Figure 3.2, has a bleed valve to remove any trapped air.

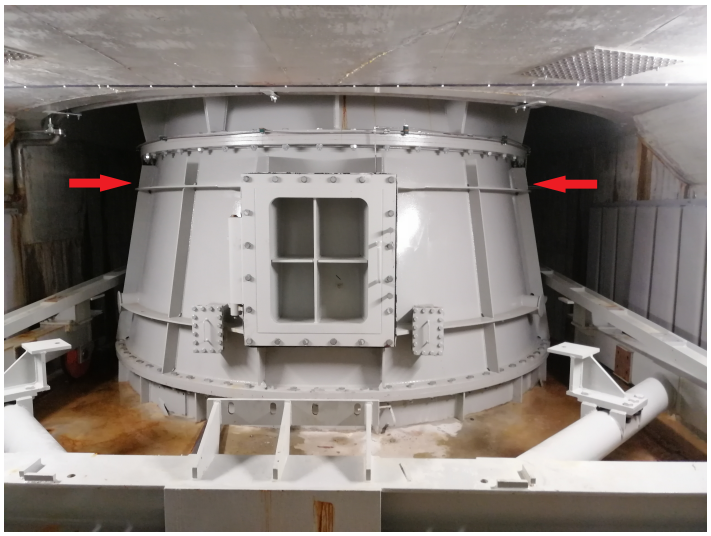

Figure 3.1: Placement of pressure sensors on the draft tube

The measurements points were chosen to get a broad spectre of the turbines operating range. The time estimate for each measurement point was set to 30 minuets. This was to give the system time to stabilize after moving the guide vanes between the operating points. The stabilizing time was set to 10 minutes. This also gave time to do more measurements if necessary. This together with the work hours for Agder Energis operator, limited the measurements to eight operating points. Due to the reservoir conditions at the day the measurement was performed, the maximum load was limited to 43 MW compared to the rated power of 44 MW. Based on that there were done measurements with an interval of 4 MW, which is presented in Table 3.1. Two measurements were done on 23 MW and 43 MW in order to validate the results.

Table 3.1: Measurement points

Measurement number	Power [MW]	Note
1	43	
2	39	BEP
3	35	
4	31	
5	27	
6	23	
7	19	
8	15	
9	23	Control point
10	23	Closed air intake
11	23	Half-closed air intake
12	43	Control point

Figure 3.2: Draft tube pressure sensor 2, with the transition piece

Figure 3.3: Inlet pressure sensor

3.2.1 Air intake

The turbine is equipped with an air intake through the shaft and into the draft tube. As a proposed solution to the noise problem, this intake was examined closer. It revealed that the air intake was already open and was sucking in a substantial amount of air. Instead of the original plan of opening and adding air, it was decided to measure the air flow in order to see how much air was sucked in. The goal for these measurements was to find an estimate of what range the air flow, and not an exact reading. For that purpose, the Schiltknecht MiniAir20 was selected, shown in Figure 3.4 together with the probe used. The location of the entrance of the air intake can be seen in Figure 3.5, and the hole used to measure the air flow can be seen in Figure 3.6. The hole was located on the floor above, approximately 7-8 m from the entrance, giving the air flow in the pipe distance to become fully developed. The air velocity was measured with the probe placed close to the centre of the pipe. Observation showed that moving the probe off centre gave little variation in velocity. Calculating the volume flow rate was done with the following equation.

$$Q = A \cdot v_{avg} \tag{3.1}$$

where A denotes the area of the pipe and v_{avg} denotes the average velocity. The air velocity measurements were done by manually recording the air flow displayed by the measurement unit. At some operating points, the air velocity varied a lot. In these cases there were approximated an average for the top and bottom values. The manual recording introduces uncertainty to the measurements.

Figure 3.4: The device used for measuring the air velocity [7].

In addition, there were done pressure measurements with closed and restricted air flow to investigate how this affected the pressure pulsations.

3.2.2 Sound recording

In between some of the measurements it was done a video recording. This was not originally plan but as it turns out the audio from the video could be used to find what audible frequencies are dominant. The recordings were done when the power

Figure 3.5: Air intake in the drain room

Figure 3.6: Hole drilled for measuring air velocity

was moving between 27 MW and 23 MW. The audio recording had a sampling rate of 44.1 kHz. Based on the analysis it is also believed that it uses a high pass filter to filter out frequencies below 40 Hz.

All equipment used during the measurements are listed in Table 3.2.

Table 3.2: List of equipment

Name	Quantity	Serial number
GE UNIK 5000 0-3 bara	2	5472337/5463597
GE UNIK 5000 0-10 bara	1	3725345
Lenovo Thinkpad	1	Logger 3
Terminal box NI-USB 6211	1	Box 3
MiniAir20	1	-

3.2.3 Data acquisition and processing

When recording the measurements, the sampling frequency was set to 5 kHz and the sampling time was set to 60 seconds. At each measuring point it was done two recordings in case it was some mistake in the reading. Since no mistakes were done, the two sequences for each measurement point where added before the FFT was executed. This creates an inconsistency in the pairing point, but is believed to be negligible. This was done to improve the quality of the result. For the measurement done with closed and half-closed air intake there where only done one recording.

For the processing, the data was transferred to MATLAB and the raw data for each sensor was put into the corresponding calibration function giving a new data set with pressure values. The pressure values were then normalized with respect to the net head of 491 kPa, before the FFT was performed.

The FFT was performed using JKWelch, which is a function in MATLAB made by Johanne Opedal Kverno. The function is based on MATLABs embedded pwelch function. For the window function the Hanning window was chosen. This is recommended in general unless low noise must be observed [25]. Together with Hanning the overlapping was set to 50% and the number of windows was set to 8. Equation 2.10 then gives a frequency resolution of 0.067 Hz. For the measurement done with restricted air flow there was done only one recording with recording time of 60 seconds. Using the same inputs in the welsh method gives a frequency resolution of 0.13 Hz

The amplitude given by the FFT was then plotted together with its frequency bin. The graphs were then analysed independently for each sensor in order to find the dominating frequencies.

3.3 Uncertainty calculations

For the calibration of the pressure sensor used for the measurements dead wight testers with two different pressure ranges were used. The low range tester is shown in Figure 3.7. Both dead weight testers have a systematic error of 0.008% provided by the instrument producer. The two sensors mounted in the draft tube were calibrated for their whole measuring range of 0-3 bara. The sensor placed at the inlet was calibrated in the range of 490 to 690 kPa. This range was based on the net head of 50 m or 491 kPa and the atmospheric pressure. Documentation for the pressure sensors can be found in Appendix E

The calibration was performed with a premade LabVIEW program. This plots the achieved uncertainty level in real time for each measuring point making it easy to see if the desired uncertainty level is reached. After each point is logged it updates the linearized plot, making it easy to discard spurious errors as the appear. The program uses a confidence interval of 95% as according to IEC 60193 [23].

Figure 3.7: Low range dead weight tester

Using Equation 2.13 with the systematic error given from the calibration instrument and the random error the total uncertainty is estimated. The result for each sensor is presented in Table 3.3. The calibration rapports can be found in Appendix D

Table 3.3: Maximum uncertainty from the calibration

Sensor	Maximum total error [%]
Inlet	0.00861
DT1	0.05978
DT2	0.04314

Chapter IV

Results

4.1 Pressure pulsations

4.1.1 General information

The design head at Iveland II is $H_0 = 50$ m or 491 kPa. The turbine is equipped with 13 runner blades and has 24 guide vanes. It operates with a rotational speed of 176.47 rpm or ∼2.94 Hz. The Best efficiency point BEP is ∼39 MW. The nominal gird frequency is 50 Hz. Table 4.1 presents the frequencies that is expected to find based on this information.

Table 4.1: Known frequencies

Name	f	f/f_n
Rotational frequency (f_n)	2.94	1
Blade passing frequency (f_r)	38.24	13
Guide vane frequency(f_g)	70.59	24
Rheingans frequency(f_p)	~ 0.82	~ 0.278
Grid frequency (f_{grid})	50	17

4.1.2 Observations during the measurements

The noise started somewhere between 31MW and 27 MW. The operator of the plant Per Olav Engen could tell that the starting point of noise varies from time to time. He suspected that this might have something to do with the water level in the river the water exits in to. Further one could also hear a significant increase in noise when moving from 27 MW to 23 MW. Apart from the noise a small movement could be seen in the draft tube when the turbine was running on part load.

4.1.3 Time series and peak to peak

The following figures presents a 10 second time series for all sensor when operating at 39 MW and 27 MW.

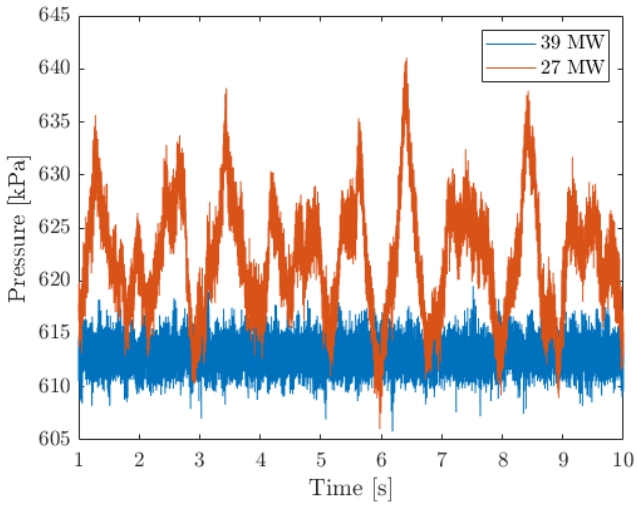

Figure 4.1: Time series from the inlet sensor.

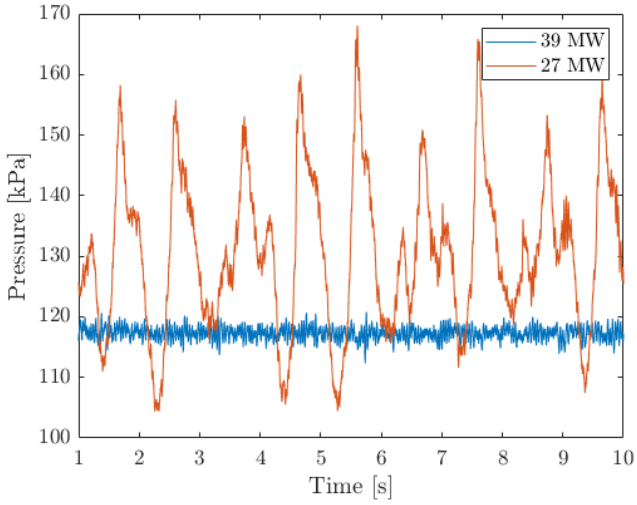

Figure 4.2: Time series from Draft tube 1.

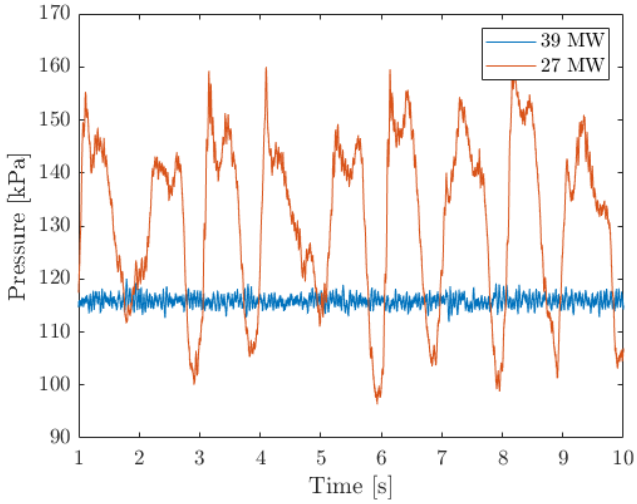

Figure 4.3: Time series from Draft tube 2.

Figure 4.4 show peak to peak values for all operating point. The peak to peak

analysis was done with 97 % confidence interval. The uncertainty bands combine the uncertainty from non-linearity, hysteresis and repeatability and i multiplied with 100. The peak to peak value is presented in kPa and as a percentage of the design head.

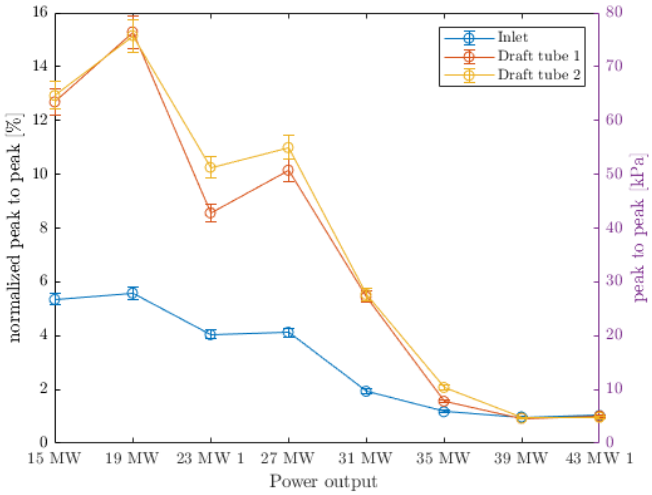

Figure 4.4: Peak to peak values for all measuring points with confidence interval of 97 %. Uncertainty band is multiplied with 100.

4.1.4 FFT analysis

The FFT performed for all sensor and measurement points are presented in Figure 4.5, 4.6 and 4.7. The frequency is normalized with the frequency of the rotational frequency of the runner and the x-axis i limited to a normalized value if 25 or $\sim$75 Hz. The power presented at each measuring point is the power output. The amplitude is normalized with the design head. The amplitude is also presented with Briggsian logarithmic scale, $log_{10}(normalized\ amplitude)$, to better show the difference in amplitude. The amplitude value is presented as percentage of the design head. Table 4.2, 4.3 and 4.4 show the dominating frequencies that are observed at each pressure sensor. Along with the frequency it shows the highest amplitude observed in measuring range, and a comment.

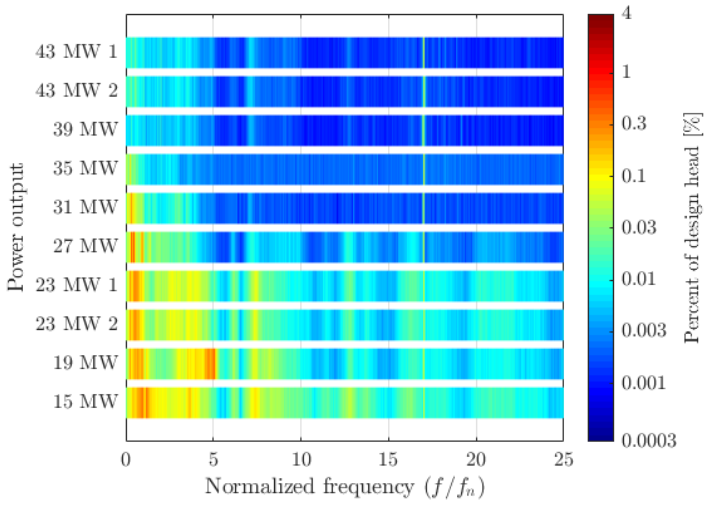

Figure 4.5: FFT for the inlet sensor. The frequency is normalized with the rotational frequency. The amplitude is normalized with the design head.

Note the change in amplitude at normalized frequency of 7.4 and 12.85 between 27 MW and 23 MW.

Table 4.2: Dominating frequencies at Inlet sensor

Normalized Frequency (f/f_n)	**Observed Frequency** $[Hz]$	**Amplitude** $[kPa]$	**Comment** $[-]$
0.22-0.33	0.66-0.99	4.42	Observed at low loads
1	2.94	0.147	Observed at high loads
2	5.88	0.0982	Observed at high loads
3	8.81	0.0982	Observed at high loads
7.40	21.75	0.6383	Observed at low loads
12.85	36.8	0.2946	Observed at low loads
17	50	0.491	Observed at all operating points

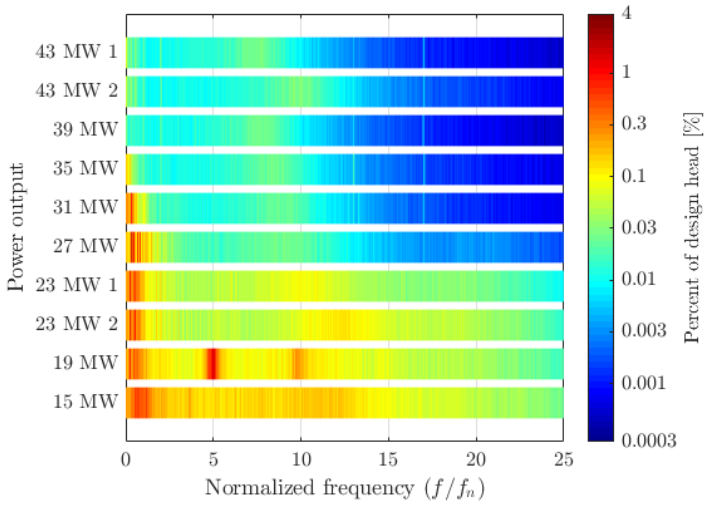

Figure 4.6: FFT for the Draft tube 1 sensor. The frequency is normalized with the rotational frequency. The amplitude is normalized with the design head.

Note the overall increase in amplitude between 27 MW and 23MW and the wide peak with a normalized value of 10 at 23 MW 1.

Table 4.3: Dominating frequencies at Draft tube sensor 1

Normalized Frequency (f/f_n)	**Observed Frequency** $[Hz]$	**Amplitude** $[kPa]$	**Comment** $[-]$
0.22-0.33	0.65-0.99	13.65	Observed at low loads
1	2.94	0.246	Observed at high loads
2	5.86	0.246	Observed at high loads
5.02	14.76	8.3	Observed at 19 MW
10.2	30	0.540	Observed at low loads
13	38.3	0.982	Observed at high loads
17	50	0.0442	Observed at high loads

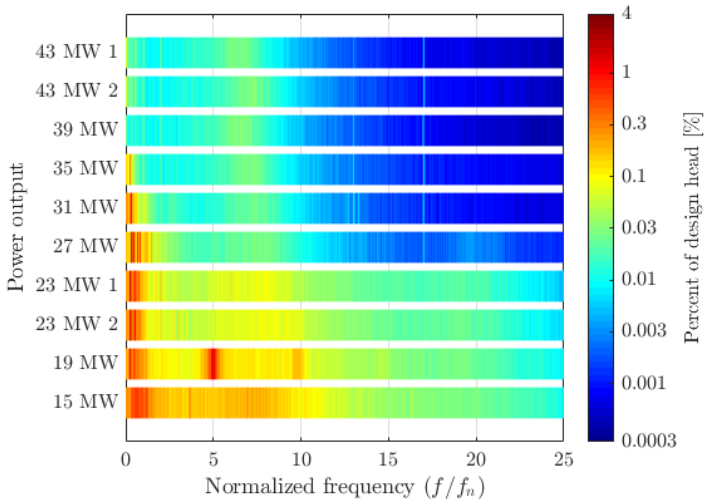

Figure 4.7: FFT for the Draft tube 2 sensor. The frequency is normalized with the rotational frequency. The amplitude is normalized with the design head.

Note the overall increase in amplitude between 27 MW and 23MW and the wide peak with a normalized value of 8.5 at 23 MW 1.

Table 4.4: Dominating frequencies at Draft tube sensor 2

Normalized Frequency (f/f_n)	**Observed Frequency** $[Hz]$	**Amplitude** $[kPa]$	**Comment** $[-]$
0.22-0.33	0.65-0.99	18.41	Observed at low loads
1	2.94	0.295	Observed at high loads
2	5.86	0.246	Observed at high loads
5.02	14.76	7.365	Observed at 19 MW
8.5	25	0.494	Observed at low loads
13	38.3	0.0412	Observed at high loads
17	50	0.0486	Observed at high loads

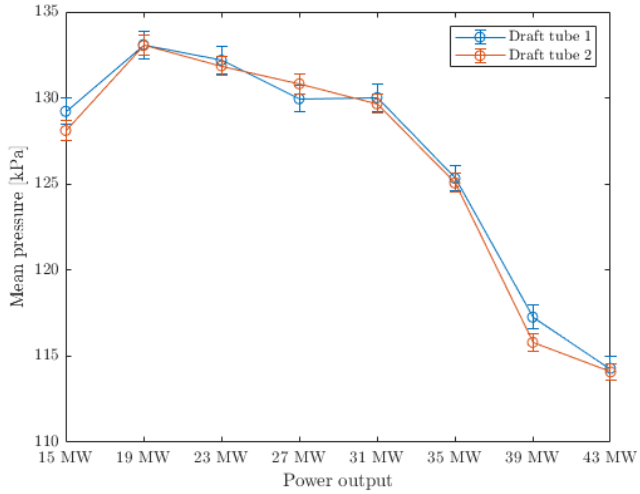

Figure 4.8: The mean pressure value for all operating points in the draft tube. the uncertainty is multiplied by 10.

4.1.5 Spectrogram of audio

When the power was reduced from 27 MW to 23 MW a video recording was made. During this transition, a significant increase in noise was observed. A spectrogram of the audio in the video recording has been performed and is presented in Figure 4.9.

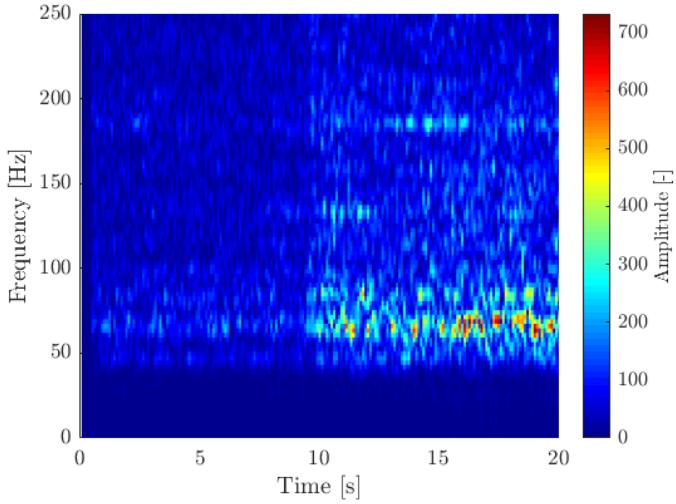

Figure 4.9: Spectrogram of sound recording 27 MW to 23 MW

Note the change in amplitude at the 10 second mark.

4.1.6 Von Kármán vortex and pressure waves in the water way

Agder Energi could not obtain drawings of the turbine. That made it difficult to examine Von Kármán vortices as a possible source of the noise. Together with Professor Dahlhaug it was decided to make some assumptions to be able to investigate these possibilities, and see if they were in the range any of frequencies found in the FFT and spectrogram.

To investigate the possible frequencies caused by Von Kármán vortices the Strouhal number is set to 0.20 and the base for the flow velocity is 10 m/s. Figure 4.10 show the result when Equation 2.3 is used with varying flow velocity and trailing edge thickness.

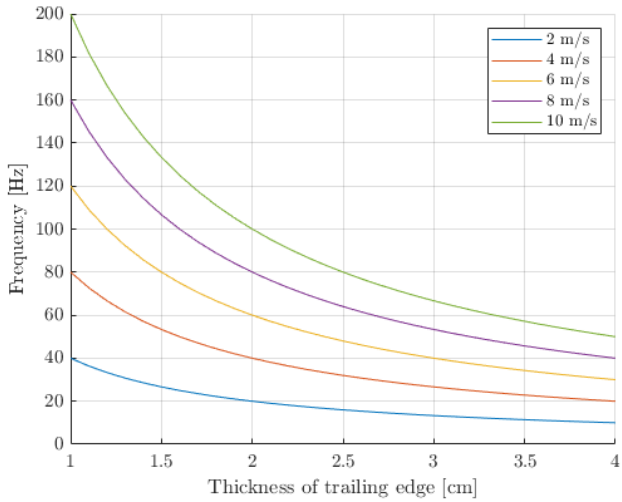

Figure 4.10: Von Kármán frequency at different trailing edge lengths and flow velocity

Another suggestion from Professor Dahlhaug was that there may be a gas cavity forming in the draft tube and that it is acting as a free water surface. Consequently there is a pressure wave moving between this surface and the nearest free water surface downstream. The nearest free water surface is an opening with an area of $27\,\mathrm{m}^2$ located in the tail race tunnel. Based drawings the distance from the draft tube to the free water surface is estimated to 35 m at normal water level in the river. The position of the gas bubble and the actual water level in the river during the measurements are not known. Therefor the distance between free water surfaces was set to vary between 25 m and 45 m. The speed of sound in water in this case is also not known and is therefore set to vary between 800 m/s and 1400 m/s. The result from using these values in Equation 2.8 is presented in Figure 4.11. Figure 4.12 presents the possible frequencies for the first harmonic $j = 2$ with the same preconditions.

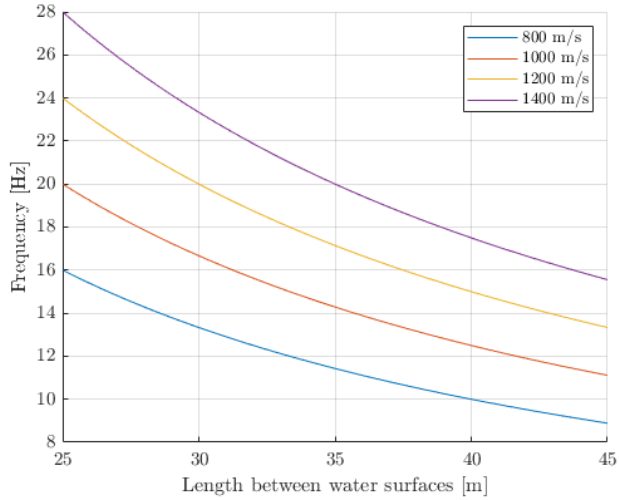

Figure 4.11: Pulsation frequency with different lengths between water surfaces and speed of sound in the water way

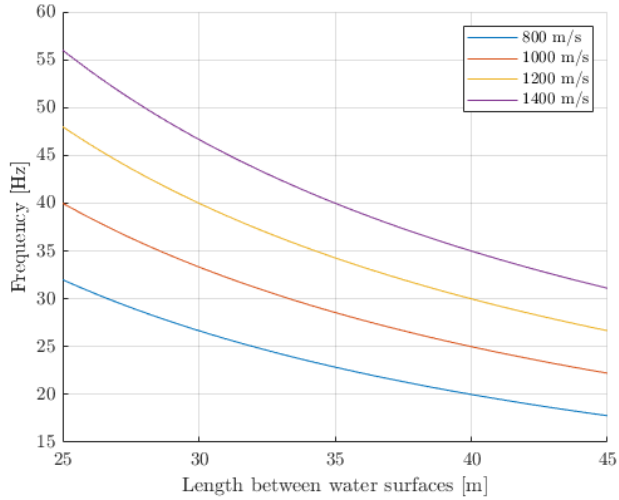

Figure 4.12: Pulsation frequency with different lengths between water surfaces and speed of sound in the water way and harmonic number $j = 2$

4.1.7 Synchronous and Asynchronous component

The result for the synchronous and asynchronous component is presented for 43 MW, 27 MW, 23 MW, 19 MW and 15 MW to show how they behave at high, part and low load. The frequency is limited to a normalized value of 25. The amplitude is normalized with the design head and presented with a Briggsian logarithmic scale.

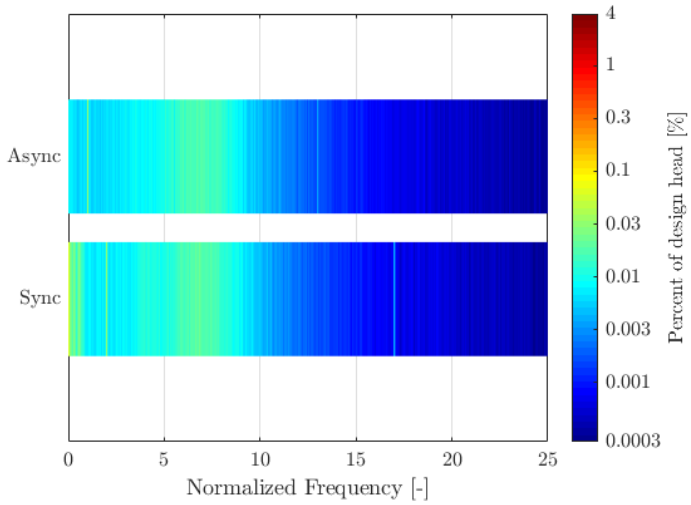

Figure 4.13: Synchronous and Asynchronous component at 43 MW

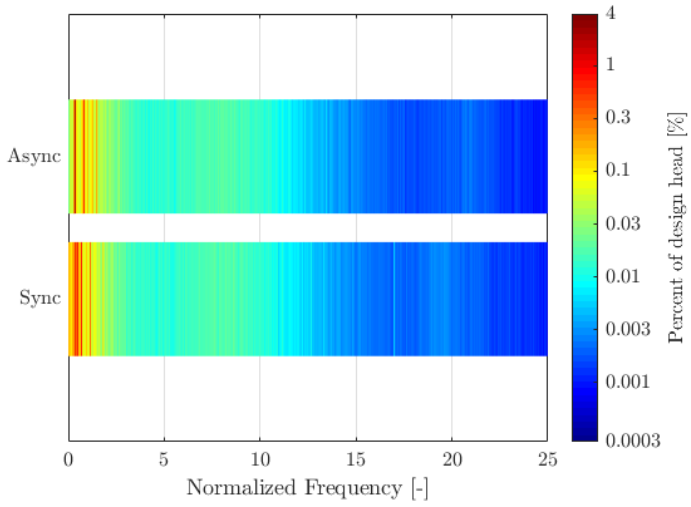

Figure 4.14: Synchronous and Asynchronous component at 27 MW

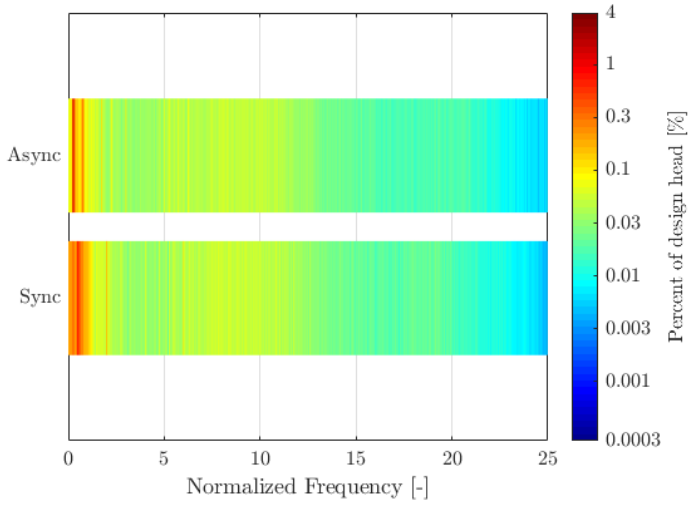

Figure 4.15: Synchronous and Asynchronous component at 23 MW

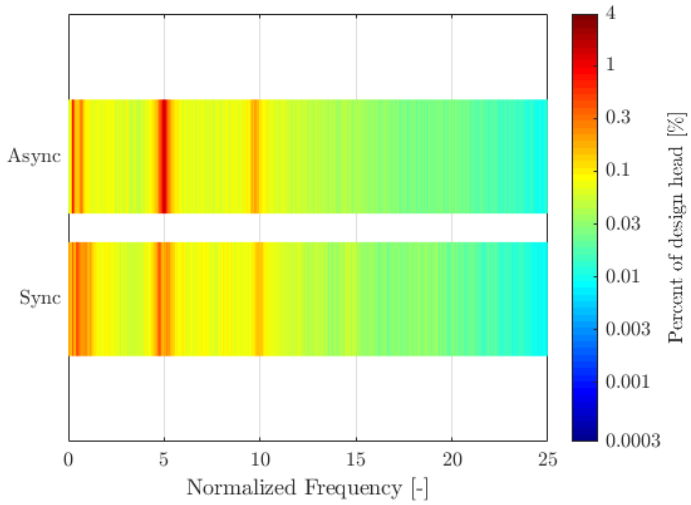

Figure 4.16: Synchronous and Asynchronous component at 19 MW

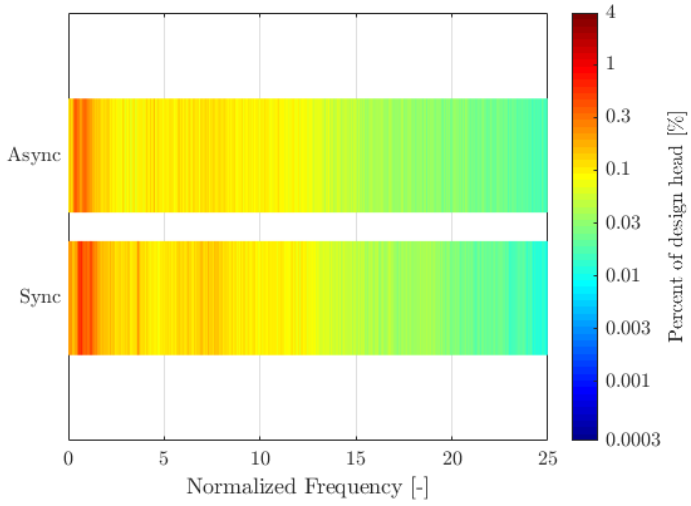

Figure 4.17: Synchronous and Asynchronous component at 15 MW

4.1.8 Air injection

One of the goals for the measurements was to investigate how the volume flow in the air intake changed at different operating points. Table 4.5 show the air velocity that was measured and the calculated air flow with the highest velocity measured at that point. The comment section shows how the flow was behaving during the measurement based on observation.

Table 4.5: Air velocity at different operating points

Power output [MW]	**Velocity** [m/s]	**Volume Flow** [m^3/s]	**Comment** [-]
43	6.3	0.15	Stable air flow
39	3.4-3.5	0.08	Stable air flow
35	0-1.5	0.03	Periodic air flow
31	7-19	0.43	Periodic air flow
27	15-24	0.54	Periodic air flow
23	7-17	0.39	Periodic air flow
19	2-5	0.11	Periodic air flow
15	0-1.5	0.03	Periodic air flow
23	7-16	0.36	Periodic air flow
23	0	0	Closed air intake
23	5-11	0.24	Half Closed air intake

Figure 4.18 show the FFT results for the measurements done with restricted air flow for Draft tube sensor 1. The amplitude is normalized with the design head and presented with a Briggsian logarithmic scale. The amplitude value is presented as percentage of the design head. The frequency range is limited to a normalized value of 25. Figure 4.19 and 4.20 show the mean value and the peak to peak value for the sensor mounted on the draft tube, respectively. The peak to peak value is presented in kPa and as a percentage of the design head. The uncertainty bands for the peak to peak values combine the uncertainty from non-linearity, hysteresis and repeatability and is multiplied with 10. The uncertainty bands for the mean values apply the total uncertainty.

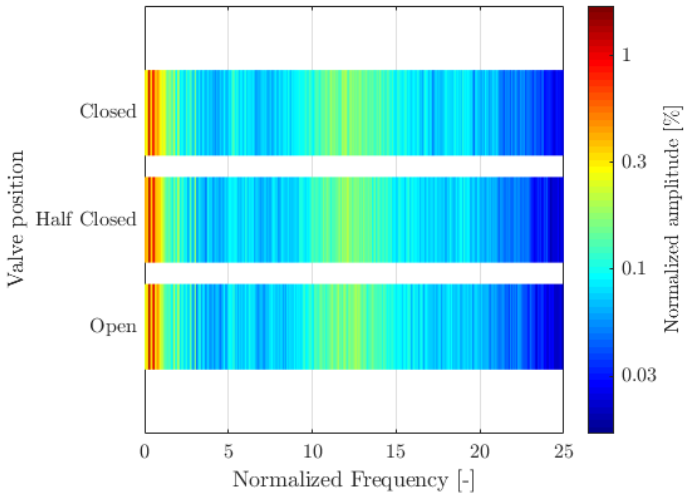

Figure 4.18: FFT at 23 MW of Draft tube sensor 1 with restricted air flow

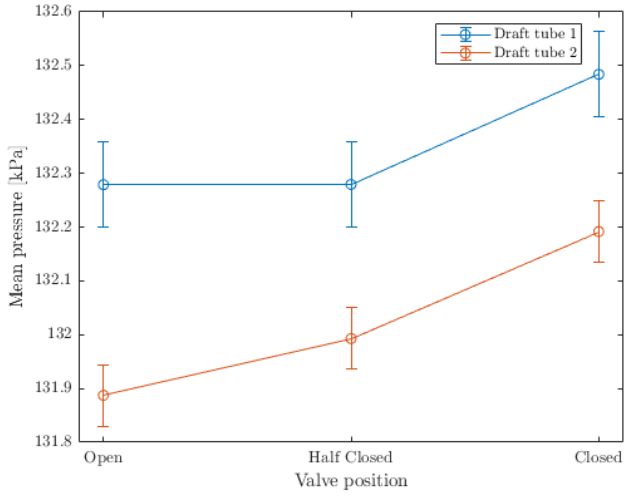

Figure 4.19: Mean values at 23 MW with restricted air flow

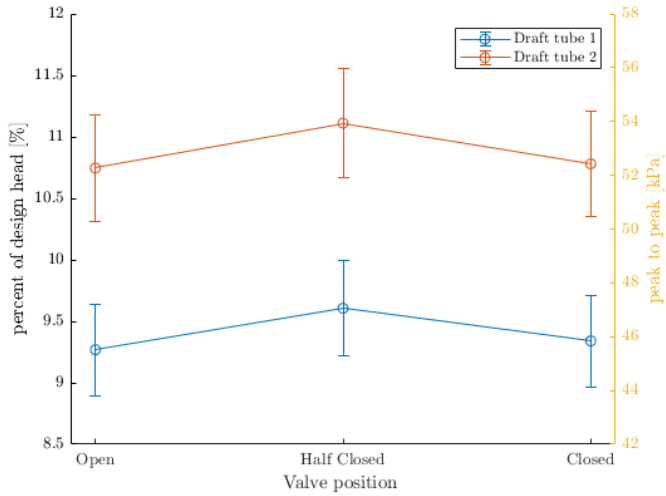

Figure 4.20: Peak to peak values at 23 MW with restricted air flow. Uncertainty is multiplied by 10

4.2 Dynamic calibrator

The final design of the dynamic calibrator is presented in Figure 4.21. All components are listen in Table 4.6. Drawings of all components can be found in Appendix B. Note that thread dimensions for the sensor and high- and low-pressure side inlets is not included. They must be adapted for the reference and calibration sensors and connections that are used for the calibration.

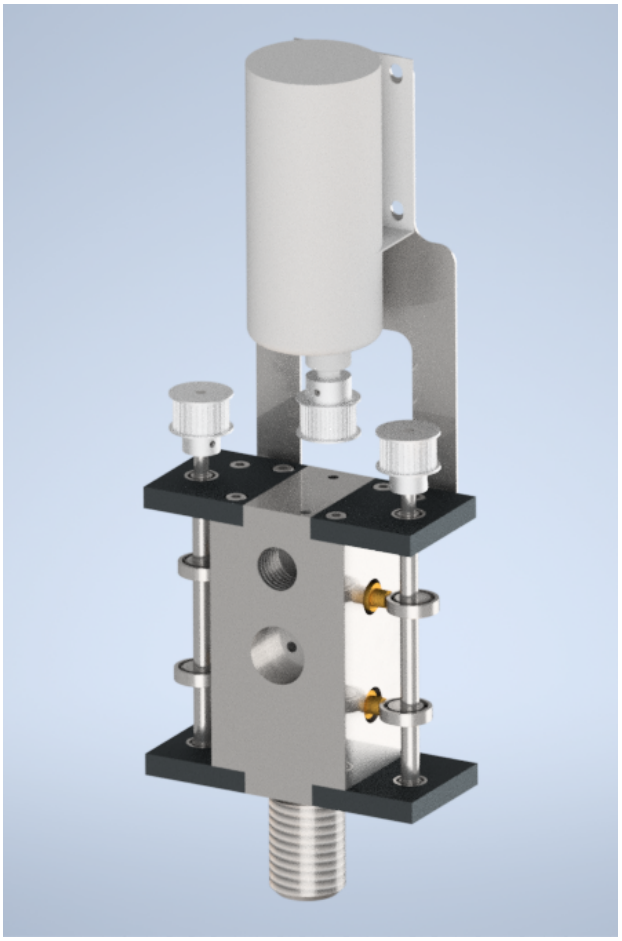

Figure 4.21: The dynamic calibrator with all its components mounted

Table 4.6: List of components for the dynamic pressure generator

Component	Quantity
Main body	1
Camshafts	2
Short pin	2
Long pin	2
Gear for camshafts	2
Gear for electric motor	1
Timing belt	1
Mount for electric motor	1
Bearing 4 mm	4
Bearing 7 mm	4
Top mount for bearings	2
Bottom mount for bearings	2
Screw M3	10
Screw M4	4
Set screw M2	3
Nut M3	2
Nut M4	4
Spring washer 3 mm	8
Washer 4 mm	8

Figure 4.22 illustrates a half section view of the main body. Showing the connection points and pressure chamber. Figure 4.23 show a half section view of the valve pins.

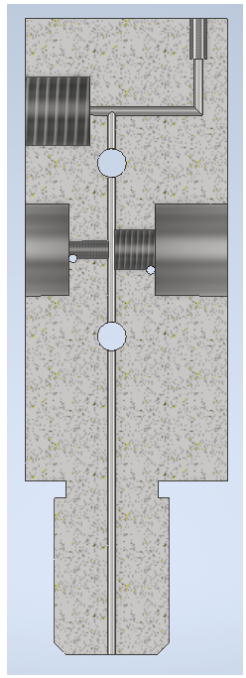

Figure 4.22: Half section view of the main body showing all inlets

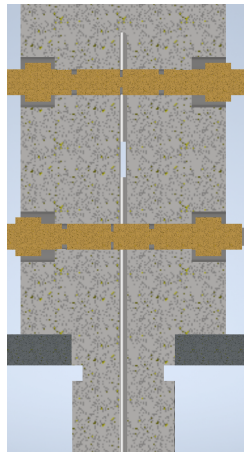

Figure 4.23: Half section view of the main body showing the valves

Chapter V

Discussion

5.1 General observations

Figure 4.1, 4.2 and 4.3 show the difference in pressure pulsations between 39 MW and 27 MW, which is BEP and the operating point with the highest pressure values respectively. Figure 4.4 show that the highest peak to peak value can be found at 19 MW with a value of 15.1 % of the design head. Figure 4.8 show that the highest mean pressure value in the draft tube is 133 kPa, also located at 19 MW.

5.2 FFT analysis

Frequencies are presented with their actual value and with the normalized values, f/f_n in parenthesise.

Figure 4.6 show low amount of pressure pulsation at 43 MW and 39 MW. At 35 MW there is a small increase at the normalized value of 0.26. This value correlates with the Rheingans frequency, f_p. A frequency in the range of 0.66-0.99 Hz (0.22-0.33) proceeds to dominate as the power is reduced, corresponding well with f_p. The amplitude increases and has its highest value at 27 MW, before it decreases as the load is reduced and at 15 MW f_p is not noticeable. It may still be present but is covered by other dominating frequencies. f_p can also be observed the inlet in Figure 4.5, though at a lower amplitude.

Looking at the high operating points at the inlet sensor in Figure 4.6 there is a spike at the normalized value of 13. This corresponds with the Blade passing frequency, f_r. Another spike can be seen at with the value of 17. This is believed to be the grid frequency, f_{grid}. Professor Ole Gunnar Dahlhaug suggested that this might be disturbance the pressure sensors which is connected to an electrical source. Both f_r and f_{grid} disappears when the power goes beneath 27 MW. This is likely due

to them drowning in other more dominating frequencies. Another frequency that can be seen at high operating points is the rotational frequency, f_n, at 2.94 Hz (1). This is visible in the draft tube and at the inlet with harmonics at 5.88 Hz (2) and 8.82 Hz (3). The values in Table 4.2, 4.3 and 4.4 show that these has relatively low amplitudes and disappears loads beneath 35 MW.

Though the Rheingans frequency is dominating the FFT-analysis it is believed not to be the source of the noise. The highest registered Rheingans frequency is 0.99 Hz, which is much lower than the audible range for humans that starts at 20 Hz. The highest amplitude is at 27 MW, but the noise is significantly louder at 23 MW-15 MW were the amplitude is lower. The noise therefore seems to behave independent from the Rheingans frequency.

As mentioned, the noise started at 27 MW and got worse at 23 MW. To investigate this the FFT-results were checked for frequencies that appear at 27 MW and increases at 23 MW. Looking at the draft tube in Figure 4.6 there is an increase in amplitude in a broad range in the transition between 27 MW to 23 MW. This range has a wide peak at around 30 Hz (10.2) at Draft tube sensor 1. The same ca be seen in Figure 4.7 for Draft tube sensor 2 but with a peak of approximately 25 Hz (8.5). Otherwise are the frequencies in the draft tube are spread out evenly, with no distinct peaks. Looking at the inlet sensor in Figure 4.5 it is possible to see different frequencies appearing at 27 MW and increasing in the transition. They can be observed at around 21.76 Hz (7.4) and 36.8 Hz (12.9).

5.3 Spectrogram of audio

The spectrogram for the audio recording of 27 MW to 23 MW is presented in Figure 4.9. It shows a clear change at around the 10 second mark. This fits well with observation done during the recording, where the noise got significantly worse in this operating area. The figure show that the dominating frequencies lies between 60 Hz to 70 Hz (20-24). It also exhibits some noise present before the abrupt change but with a lower amplitude. This correlates to the frequency band that can be seen at the inlet in Figure 4.5 with normalized values of 20-24. Under 40 Hz there seems to be no activity because the audio recorder is using a high pass filter that excludes frequencies under 40 Hz. Since the audible range for humans is 20 Hz it might be frequencies that are of importance in this area. Comparing the frequency in the spectrogram with the FFT of the draft tube it is possible that the 60-70 frequency band is a second harmonic to the wide peak at 30 Hz (10.2) seen in Figure 4.6.

Since the audio was not originally planned it exhibits some shortcomings for instance is how the power changed during the recording not known. The recording device also limits the lower frequency range, leaving out frequencies that could be

significant.

5.4 Von Kármán vortices and pressure waves in the waterway

Figure 4.10 show that the Von Kármán frequency correspond to the frequencies discussed in Section 5.2 and 5.3 for low flow velocities. As the trailing edge thickness increases, higher flow velocities approach the same frequency range. This indicates that Von Kármán can be the source of the noise and needs to be examined further. Equation 2.3 show that the frequency will change with different velocity. One way to investigate if Von Kármán vortices is indeed the source may be to conduct sound recordings at different operating points to see if any change in the frequency.

Figure 4.11 show that the frequency of the pressure wave moving between the draft tube and the free surface lie in the range of 21.76 Hz (7.4) observed at the inlet. Further it is also in the range of the 30 Hz (10.2) and 25 Hz (8.5) observed in the draft tube. Figure 4.12 with the harmonic number $j = 2$, the 36.8 Hz (12.9) is also included in possible frequency range. If the gas bubble in the draft tube exists and is a result of cavitation it could explain why the starting point of the noise varies. When the water level in the river varies, the conditions for cavitation in the draft tube changes. This corresponds with the observation made by the plant operator. The observation of the varying starting point of the noise and the frequencies found in Figure 4.11 and 4.12, indicate that pressure waves in the water way may be a possible source for the noise. The pressure wave does not necessarily create the noise on its own but it may achieve resonance condition with some unknown structural or mechanical part of the plant.

5.5 Synchronous and Asynchronous component

The analysis of the synchronous and asynchronous pressure component was based on a selection of all operating points

At 43 MW, Figure 4.13, and 15 MW , Figure 4.17, it is the synchronous component that is dominant. Further at part load in Figure 4.14 and 4.15 the asynchronous component is dominant. As for 30 Hz (10.2) mentioned in Section 5.2, there is no significant difference in the two components at the various operating points.

The operating point 19 MW with the unknown frequency 14.76 Hz (5) is represented in Figure 4.16. The figure show that this is clearly an asynchronous phenomenon.

5.6 Air injection

Table 4.5 presents the air velocity in the air intake for each measuring point. It shows that the air flow varies a lot between the different operating points. At some operating point the air flow also varies at the individual operating point. Based on observations done during the measurement the change in flow seemed to be periodical. Since the recording was done visually it is not possible to find how the cycle behaves and compare it to other phenomena found in the pressure measurements. The flow appears to be stable with little fluctuations when running at high loads. At 35 MW the flow starts to behave in a periodic manner but there is almost no air flow. At 31 MW there is a drastic change in air velocity and fluctuations. The highest air velocity is found at 27 MW with it fluctuating between 15-24 m/s. After that, the air flow decreases and at 15 MW it is close to zero.

Comparing the air flow to where the Rheingans frequency is dominating there appears to be a link. Considering the amplitude there is also a similarity in how it behaves compared with the air velocity. Both start low at 35 MW with a peak at 27 MW, before decreasing towards 15 MW.

The FFT in Figure 4.18 show that there is little difference between the measuring points with various air flow. The peak to peak values in Figure 4.20 show no consistent change with the reduction in air flow. Figure 4.19 has a small increase as the air flow is reduced. No significant change in noise level was observed during the measurements.

5.7 Dynamic Calibrator

The base for the design of the dynamic calibrator illustrated in Figure 4.21 is a periodic pressure generator with constant volume and varying mass in the pressure chamber. This is achieved by using fast acting valves operated by camshafts. The camshaft is connected to a timing belt powered by a electric motor with variable speed. The variable speed makes it possible to change the frequency of the applied pressure.

Figure 4.22 shows access points for the calibration and the reference sensor in the middle. At the bottom of the treads there are drainage holes. This makes it easier to spot leakage coming from the treads. The threaded hole at the top left side is the access point for the low-pressure source while the bottom piece is to be connected to the high-pressure source. The two holes intersecting the line to the chamber is where the pins separating the two pressure sides is located. At the top there is an access point for a bleed valve. The chamber is designed so the reference and calibration sensor is mounted close together in order minimise the difference in the

sensed pressure. The chamber itself is small so its natural frequency is kept far above the operating range of the calibrator.

The pins shown in Figure 4.23 has a groove which gives the pressure chamber alternating access to the low- and high-pressure source as the pins are operated. The pins are designed so that the open pressure side closes before the other one opens. Both sides of the pins has two grooves, so rubber gaskets can be fitted. The pins are divided in two pieces so they can be mounted from each side. This is done because experience has shown that mounting it from one side would tear the rubber gasket.

Chapter VI

Conclusion

The pressure measurement at Iveland II was executed successfully under good conditions. Further the measurement data was processed in MATLAB that provided suitable material for further analysis.

The FFT analysis showed that the Rheingans is dominant both at the inlet and in the draft tube when operating at part load. Its low frequency of $\sim$ 1 Hz ruled it out as a possible noise source. The noise started at 27 MW and increased when moving to 23 MW. The FFT where examined for frequencies that appear in this transition. At the inlet one could find the frequencies 21.76 Hz (7.4), 36.8 Hz (12.9) and 60-70 Hz (20-24). At the draft tube, a wide peak at 30 Hz (10.2) and 25 Hz (8.5) could be observed at Draft tube sensor 1 and 2, respectively. A spectrogram of an audio recording showed that the sound lies in the range of 60-70 Hz.

By comparing the observed frequencies with the possible pressure pulsation sources some hypotheses were developed towards the cause of the noise and vibrations but it did not lead to a conclusion.

Based on simple calculations possible frequencies caused by Von Kármán vortecies were found to be in the range of the frequencies mentioned above. Further investigation is necessary to determine if this is the source.

The investigation of a gas bubble acting as a free water surface in the draft tube revealed it as a potential source. Calculations done for a pressure waves moving between two free water surfaces based on the length to the nearest free water surface, revealed that the possible frequencies found were in the range of all the different frequencies observed at the inlet and in the draft tube. A gas bubble caused by cavitation could also explain why the starting point of the noise varies with the water level in the river down stream. These different observations strengthen the possibility of pressure waves in the water way being the source of the noise and

vibrations. The measurements conducted in this thesis are not enough to conclude.

Restricting the air flow entering the draft tube through the turbine shaft proved to have little effect on the pressure pulsations.

A dynamic calibration device was designed but was not manufactured. Quality assurance is necessary before the device is produced. Since the calibrator was not finished no dynamic calibration was performed on the pressure sensors used at Iveland II.

Chapter VII

Further work

To further investigate the possibility of Von Kármán vortices being the cause of the noise, it would be an advantage to obtain the drawings of the stay vanes, guide vanes and the turbine blades. With the design established it is possible to use more accurate equations to determine a more accurate estimate of the frequency range.

It is also recommended to conduct more accurate sound measurements with a device that covers the range of possible frequencies. Sound measurements should then be performed for both transient and at steady state operation.

For the dynamic calibrator there are some aspects that needs to decided before the device can be sent for machining. It is necessary to pick a reference and calibration senor so the thread dimensions at each inlet can be made to fit. The same applies for the inlet for the high-and low-pressure sides. Further the parts must be quality assured and tolerances must be added for the dimensions.

References

[1] Iveland kraftstasjon | Våre vannkraftverk | Vannkraft | Produksjon | Vår virksomhet, https://www.ae.no/var-virksomhet/produksjon/vannkraft/vare-vannkraftverk/iveland-kraftstasjon/ (2020).

[2] Agder Energi, Iveland kraftverk, https://www.ae.no/virksomhet/vannkraft/kraftstasjoner/iveland-kraftstasjon/, Last accessed on 2019-11-04 (2018).

[3] E. Agnalt, Rotor Stator Interaction in Low- Specific Speed Francis Turbines (2019).

[4] P. Dörfler, M. Sick, A. Coutu, Flow-Induced Pulsation and Vibration in Hydroelectric Machinery: Engineer's Guidebook for Planning, Design and Troubleshooting (2013). doi:10.1007/978-1-4471-4252-2.

[5] P. J. Gogstad, Experimental investigation and mitigation of pressure pulsations in Francis turbines (2017).

[6] J. O. Kverno, V. S. Ulvan, Pressure pulsations and thermodynamic efficiency measurements at Smeland power plant (2018).

[7] Yumpu.com, MiniAir 20 Portable Vane Anemometer with Display - Omni Instruments, https://www.yumpu.com/en/document/read/34575004/miniair-20-portable-vane-anemometer-with-display-omni-instruments.

[8] E. Kobro, Measurement of Pressure Pulsations in Francis Turbines (2010).

[9] C. Bergan, Transient LDA Measurements in the Draft Tube of a High Head Francis Turbine 81 (2014).

[10] I. Iliev, Francis turbines for variable speed operation (2020).

[11] E. Røneid, Pressure pulsations at Iveland Power Plant (Dec. 2019).

[12] D. B. Sannes, Pressure Pulsation and Stresses in a Francis Turbine Operating at Variable Speed (2018).

[13] H. Ormestad, Egenfrekvens, Store norske leksikon (May 2017).

[14] A-to-Z Guide to Thermodynamics, Heat and Mass Transfer, and Fluids Engineering: AtoZ V (2006).

[15] H. H. Francke, Increasing Hydro Turbine Operation Range and Efficiencies Using Water Injection in Draft Tubes (2010).

[16] Torbjørn Nielsen, Dynamisk dimensjonering av vannkraftverk (1990).

[17] T. Lindseth Bergfløtdt, Development of an accumulator system for a pulsating Pelton nozzle (2017).

[18] B. A. Olshausen, Aliasing (2000).

[19] G. Heinzel, A. Rüdiger, R. Schilling, Spectrum and spectral density estimation by the Discrete Fourier transform (DFT), including a comprehensive list of window functions and some new flat-top windows, Max Plank Inst 12 (Jan. 2002).

[20] J.Marsar, Improving FFT Resoltuion (Feb. 2015).

[21] T. Platte, M. Iwanczik, M. Mende, Dynamic Pressure Transducer Calibration – Traceable? 14003 (2017). doi:10.1051/metrology/201714003.

[22] Guide for the Dynamic Calibration of pressure transducers (2002).

[23] NEK IEC 60193:2019 (2019).

[24] B. W. Solemslie, Compendium in Instrumentation, Calibration & Uncertainty Analysis (2010).

[25] H. Schmid, How to use the FFT and Matlab's pwelch function for signal and noise simulations and measurements 13 (2012).

Appendix A

Health, Safety and Environment

A.1 Job Safety Analysis

NTNU HMS	Kartlegging av risikofylt aktivitet	Utarbeidet av	Nummer	Dato	
		HMS-avd.	HMSRV2601	22.03.2011	
		Godkjent av		Erstatter	
		Rektor		01.12.2006	

Enhet: **EPT/IVT-NTNU** **Dato: 06.02.2020**

Linjeleder:

Deltakere ved kartleggingen (m/ funksjon)**: Bjørn Winther Solemlie, ansv. veileder, Erlend Røneid, student**
(Ansv. veileder, student, evt. medveiledere, evt. andre m. kompetanse)

Kort beskrivelse av hovedaktivitet/hovedprosess: Masteroppgave student Erlend Røneid. Trykkpulsasjoner ved Iveland kraftverk.

Er oppgaven rent teoretisk? (JA/NEI)**: Nei** *«JA» betyr at veileder innestår for at oppgaven ikke inneholder noen aktiviteter som krever risikovurdering. Dersom «JA»: Beskriv kort aktiviteteten i kartleggingskjemaet under. Risikovurdering trenger ikke å fylles ut.*

Signaturer: *Ansvarlig veileder:* Bjørn Winther Solemlie *Student:* Erlend R.

ID nr.	Aktivitet/prosess	Ansvarlig	Eksisterende dokumentasjon	Eksisterende sikringstiltak	Lov, forskrift o.l.	Kommentar
1	Transport				Vegtrafikkloven	
2	Montere/Demontere pitot tube	Agder Energi		Påbudt verneutstyr		
3	Montere/Demontere trykksensorer	Agder Energi		Påbudt verneutstyr		
4	Utføre målinger	Agder Energi		Påbudt verneutstyr		

NTNU HMS	Risikovurdering	Utarbeidet av	Nummer	Dato
		HMS-avd.	HMSRV2603	22.03.2011
		Godkjent av		Erstatter
		Rektor		01.12.2006

Enhet: **EPT/IVT-NTNU** **Dato: 06.02.2020**

Linjeleder:

Deltakere ved kartleggingen (m/ funksjon): Bjørn Winther Solemlie, ansv. veileder, Erlend Røneid, student
(Ansv. Veileder, student, evt. medveiledere, evt. andre m. kompetanse)

Risikovurderingen gjelder hovedaktivitet: Masteroppgave student Erlend Røneid. Trykkpulsasjoner ved Iveland kraftverk.

Signaturer: *Ansvarlig veileder:* Bjørn Winther Solemlie *Student:* E. Røneid.

ID nr	Aktivitet fra kartleggings-skjemaet	Mulig uønsket hendelse/ belastning	Vurdering av sannsyn-lighet	Vurdering av konsekvens:				Risiko-Verdi (menn-eske)	Kommentarer/status Forslag til tiltak
			(1-5)	Menneske (A-E)	Ytre miljø (A-E)	Øk/ materiell (A-E)	Om-dømme (A-E)		
2	Montere/Demontere pitot tube	Fall frå høgde	2	B	A	A	A	B2	Bruke påbudt verneutstyr
2	Montere/Demontere pitot tube	Augeskade	2	C	A	A	A	C2	Bruke vernebriller
3	Montere/Demontere trykksensorer	Sklifare	2	B	A	A	A	B2	Bruke påbudt verneutstyr
4	Utføre målinger	Hørselsskade	3	C	A	A	A	C3	Bruke hørselsvern, ikkje oppholde seg i støysona over lengre tid
1	Transport	Bilulykke	1	E	A	A	B	D1	Bruke bilbelte, kjøre etter forholda
1	Transport	Flyulykke	1	E	B	B	A	E1	Følge sikkerhetsinstruks

Sannsynlighet vurderes etter følgende kriterier:

Svært liten 1	Liten 2	Middels 3	Stor 4	Svært stor 5
1 gang pr 50 år eller sjeldnere	1 gang pr 10 år eller sjeldnere	1 gang pr år eller sjeldnere	1 gang pr måned eller sjeldnere	Skjer ukentlig

Konsekvens vurderes etter følgende kriterier:

Gradering	Menneske	Ytre miljø Vann, jord og luft	Øk/materiell	Omdømme
E Svært Alvorlig	Død	Svært langvarig og ikke reversibel skade	Drifts- eller aktivitetsstans >1 år.	Troverdighet og respekt betydelig og varig svekket
D Alvorlig	Alvorlig personskade. Mulig uførhet.	Langvarig skade. Lang restitusjonstid	Driftsstans > ½ år Aktivitetsstans i opp til 1 år	Troverdighet og respekt betydelig svekket
C Moderat	Alvorlig personskade.	Mindre skade og lang restitusjonstid	Drifts- eller aktivitetsstans < 1 mnd	Troverdighet og respekt svekket
B Liten	Skade som krever medisinsk behandling	Mindre skade og kort restitusjonstid	Drifts- eller aktivitetsstans < 1uke	Negativ påvirkning på troverdighet og respekt
A Svært liten	Skade som krever førstehjelp	Ubetydelig skade og kort restitusjonstid	Drifts- eller aktivitetsstans < 1dag	Liten påvirkning på troverdighet og respekt

Risikoverdi = Sannsynlighet x Konsekvens
Beregn risikoverdi for Menneske. Enheten vurderer selv om de i tillegg vil beregne risikoverdi for Ytre miljø, Økonomi/materiell og Omdømme. I så fall beregnes disse hver for seg.

Til kolonnen "Kommentarer/status, forslag til forebyggende og korrigerende tiltak":
Tiltak kan påvirke både sannsynlighet og konsekvens. Prioriter tiltak som kan forhindre at hendelsen inntreffer, dvs. sannsynlighetsreduserende tiltak foran skjerpet beredskap, dvs. konsekvensreduserende tiltak.

A.2 Communication plan

Plan for kommunikasjon ved reise til Iveland Kraftverk, 18.02-20.02

Ved en eventuell uønsket hendelse kontakt NTNU:

Instituttleder: Terese Løvås +47-91897007/+47/73593709

Dekanus: Olav Bolland +47-91897209/ +47-73591604

Faglig ansvarlig: Bjørn Winther Solemslie +47-93212395

Nødnummer»

Brann: 110

Politi: 112

Helse: 113

Husk å oppgi:

- Hvem du er
- Hva som har skjedd
- Hvor skade/ulykkessted er

Beredsskapstelefon NTNU:

Ved ulykker eller dødsfall i utlandet, vil nummeret til vaktselskapet **+47 800 80 388** kunne ringes fra utlandet. Siemens Building Technologies AS vil da varsle nøkkelpersoner ved NTNU.

Deltagere:

Erlend Røneid **tlf: +47/97105915**

Bård Brandåstrø **tlf: +47/ 91897257**

Contact Persons:

S.N	First names	Last name	Company	E-mail	Phone
1	Bjørn	Winther Solemslie	NTNU	bjorn.w.solemslie@ntnu.no	+47 93212395
2	Erlend	Røneid	NTNU	erleron@stud.ntnu.no	+47 97105915
3	Bård	Brandåstrø	NTNU	Bard.brandastro@ntnu.no	+47 91897257

Reiserute:

DY0741: TRD – OSL, 18/02 kl 06.30

DY0270: OSL – KRS, 18/02 kl 07.30

SK0222: KRS – OSL, 20/02 kl 18.15

SK0370: OSL – TRD, 20/02 kl 19.35

Appendix B

Drawings of Dynamic calibrator

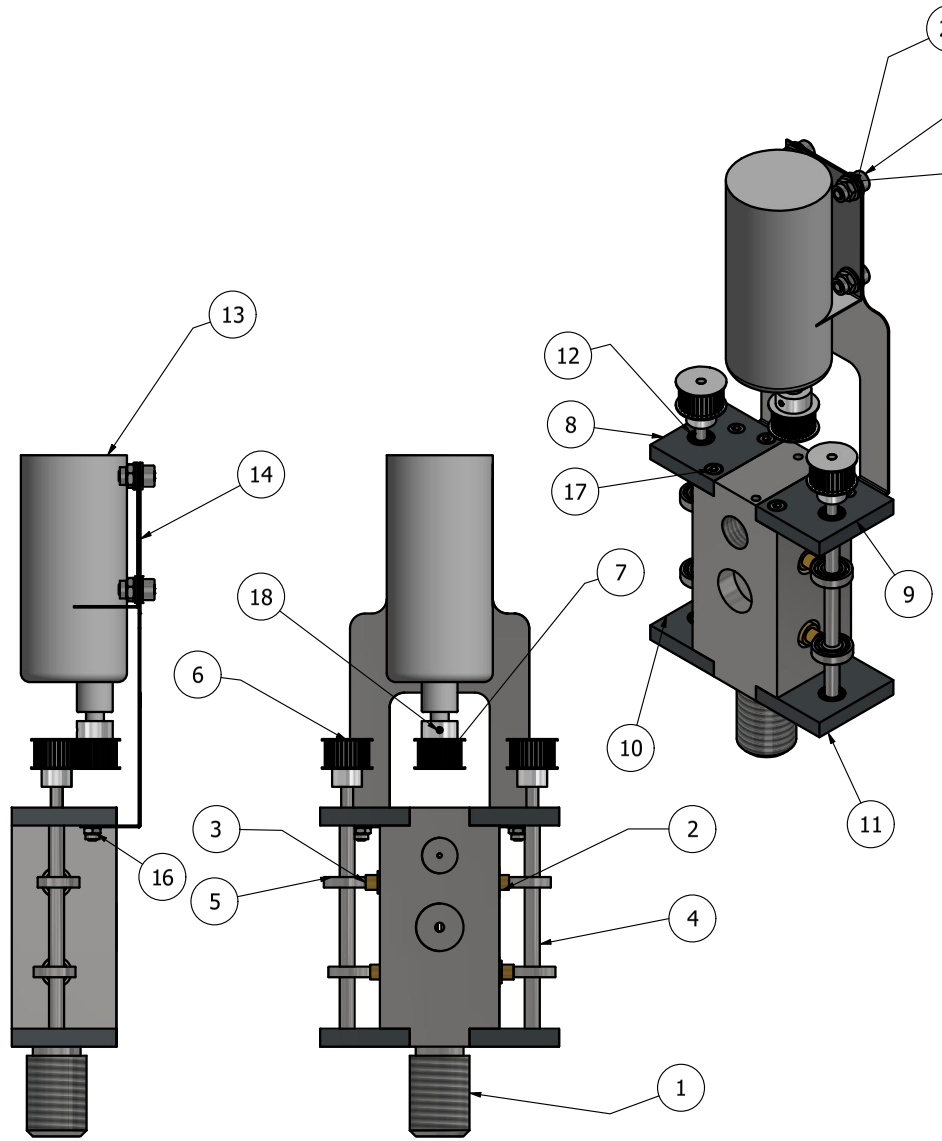

PARTS LIST			
ITEM	QTY	PART NUMBER	DESCRIPTION
1	1	Main Body	
2	2	Long pin	
3	2	Short pin	
4	2	Camshaft	
5	4	BS 290 - SKF 618/7	Single row ball bearings
6	2	Gear camshaft	
7	1	Gear electric motor	
8	1	Top bearing mount	
9	1	Top bearing mount (mirror item 8)	
10	1	Bottom bearing mount	
11	1	Bottom bearing mount (mirror item 10)	
12	4	BS 290 - SKF 618/4	Single row ball bearings
13	1	Electric motor	
14	1	Mount electric motor	
15	8	CNS 161 - A - 3	Spring Washer
16	2	DIN 985 - M3	Hex Nut
17	10	AS 1420 - 1973 - M3 x 8	ISO metric hexagon socket head cap screws
18	3	ANSI B18.3.6M - M2x0,4 x 3, BHSSSFPM	Broached Hexagon Socket Set Screw - Flat Point
19	4	AS 1420 - 1973 - M4 x 8	ISO metric hexagon socket head cap screws
20	4	DIN 985 - M4	Hex Nut
21	8	CNS 4407 - 3,6mm	Crinkle Washer

Designed by	Checked by	Approved by	Date	Date	
Erlend Røneid				26.06.2020	

Dynamic calibrator

DC assembled

Edition

Sheet 1 / 1

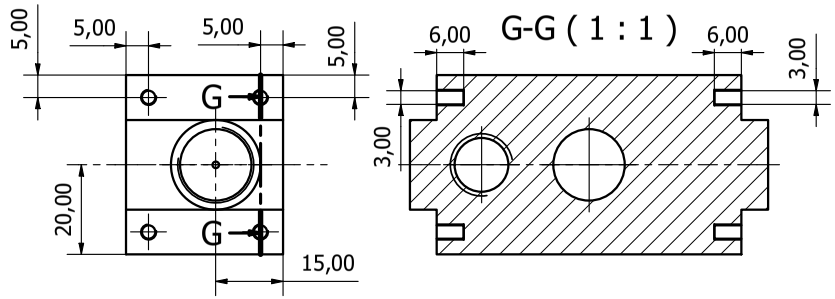

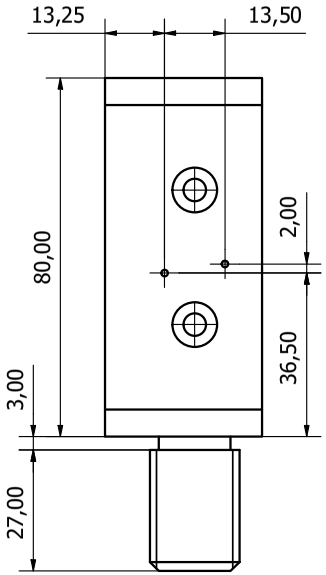

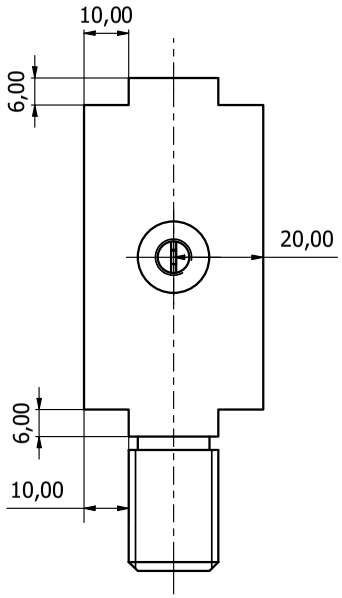

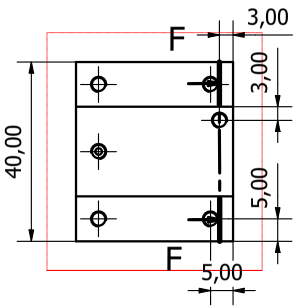

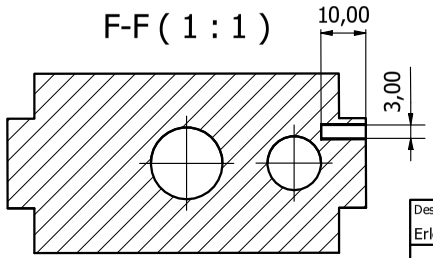

Designed by	Checked by	Approved by	Date	Date	
Erlend Røneid				25.06.2020	

	Dynamic calibrator		
Main body		Edition	Sheet 1 / 2

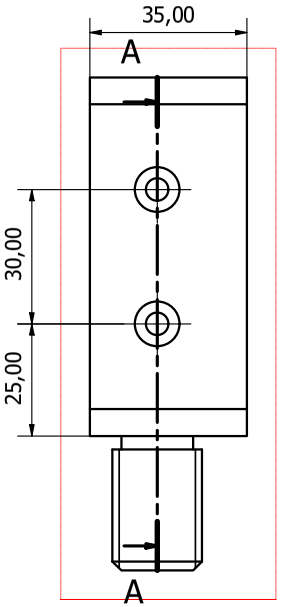

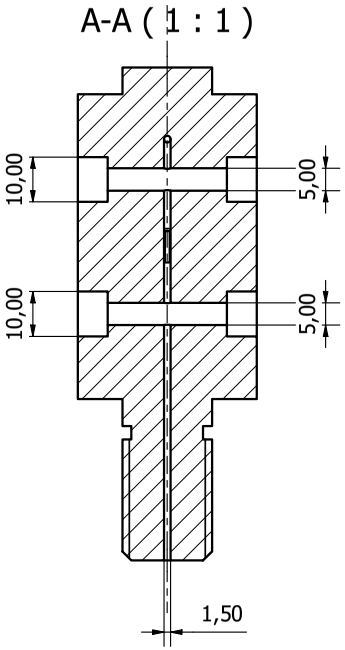

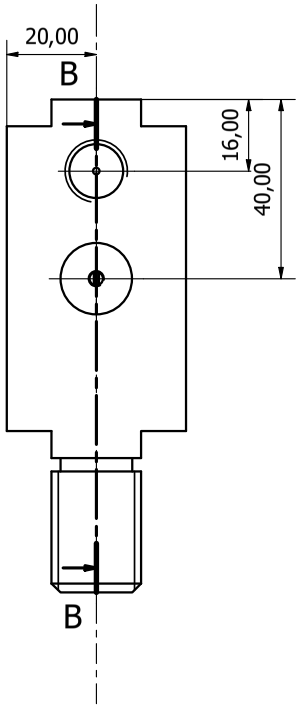

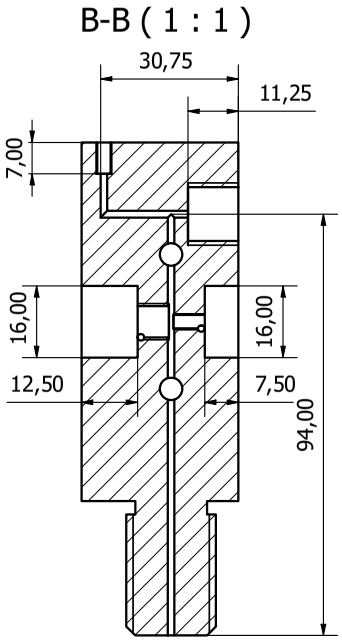

Designed by	Checked by	Approved by	Date	Date	
Erlend Røneid				25.06.2020	

	Dynamic calibrator		
	Main body	Edition	Sheet 2 / 2

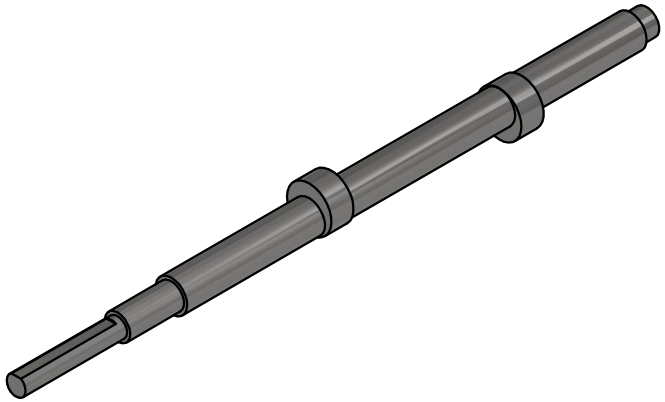

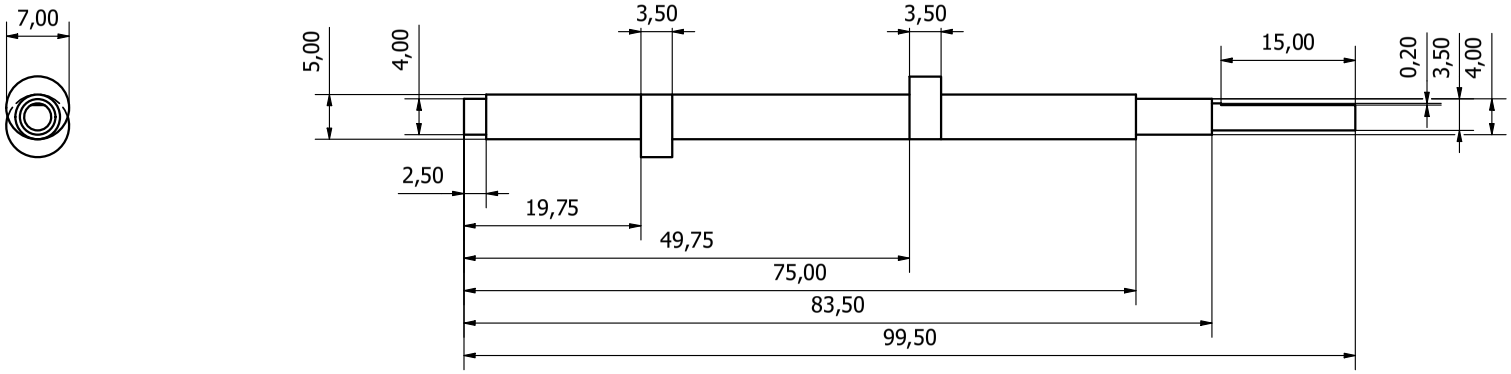

Designed by	Checked by	Approved by	Date	Date	
Erlend Røneid				25.06.2020	

Dynamic calibrator

Camshaft

Edition

Sheet 1 / 1

A-A (2 : 1)

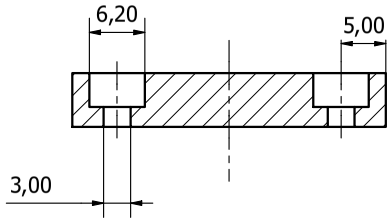

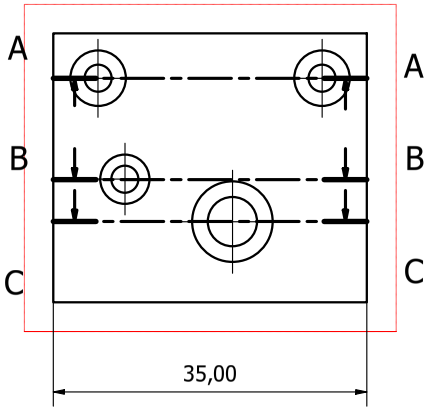

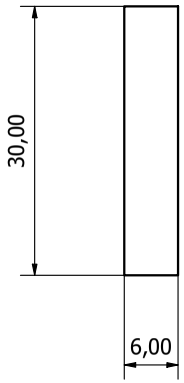

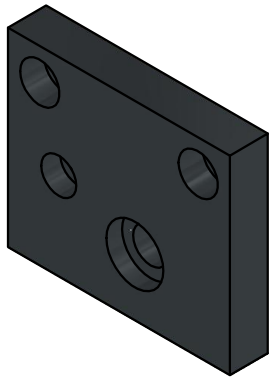

C-C (2 : 1)

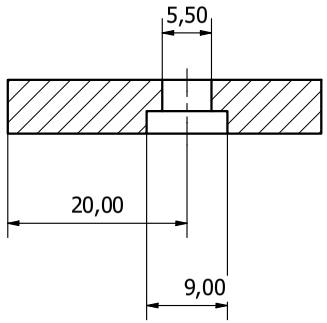

B-B (2 : 1)

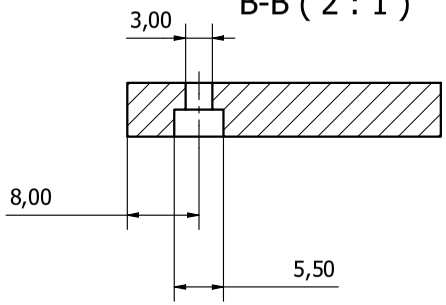

Designed by	Checked by	Approved by	Date	Date	
Erlend Røneid				26.06.2020	

Dynamic calibration

Top bearing mount

Edition

Sheet 1 / 1

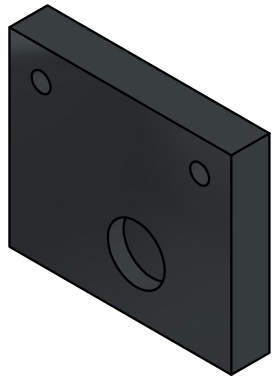

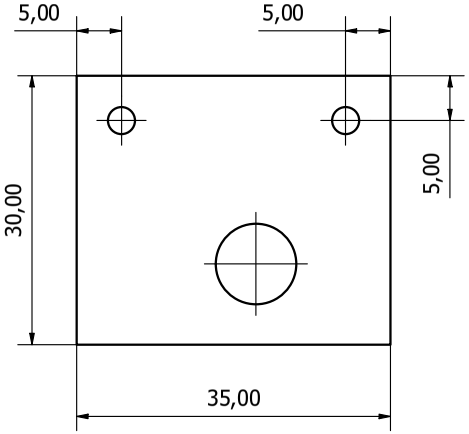

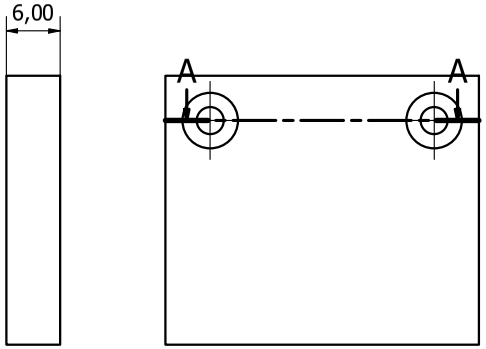

A-A (2 : 1)

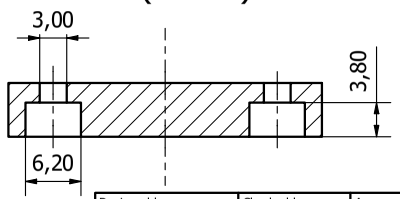

Designed by	Checked by	Approved by	Date	Date	
Erlend Røneid				26.06.2020	

	Dynamic calibrator		
	Bottom bearing mount	Edition	Sheet 1 / 1

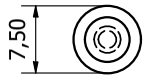

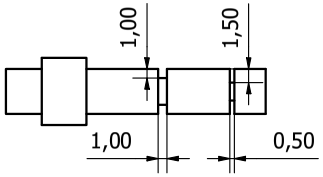

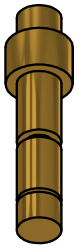

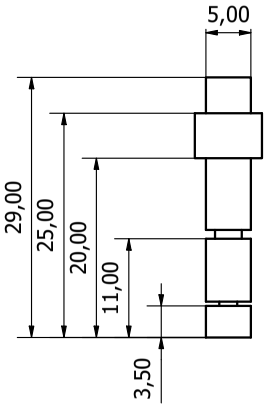

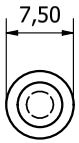

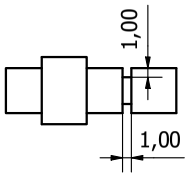

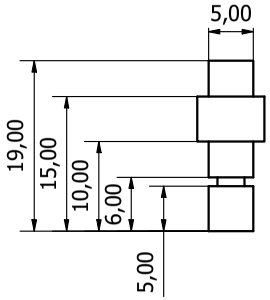

Designed by	Checked by	Approved by	Date	Date	
Erlend Røneid				25.06.2020	

	Dynamic calibrator		
	Pins	Edition	Sheet 1 / 1

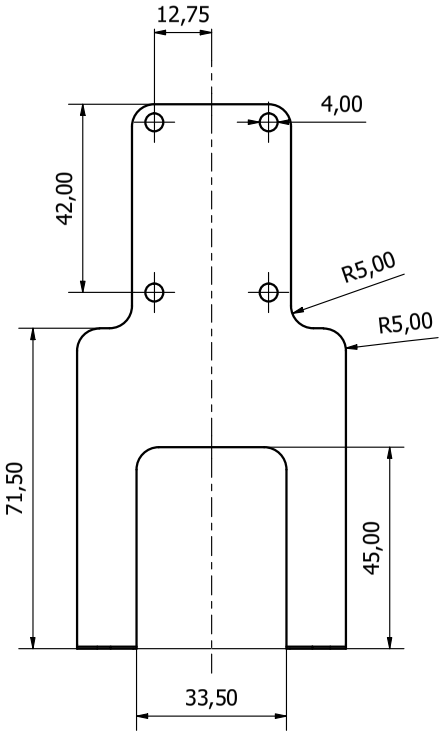

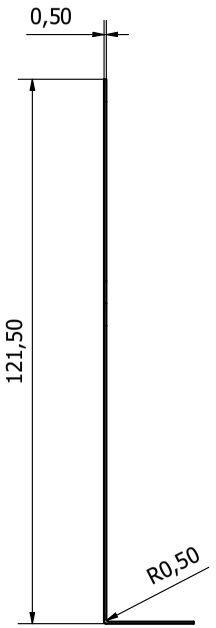

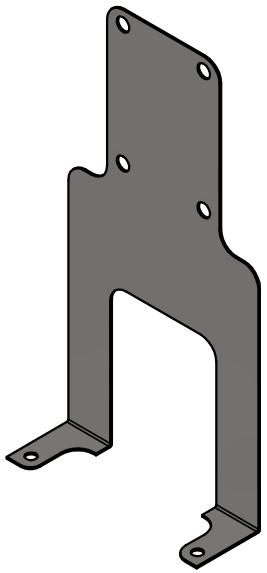

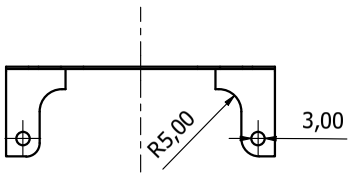

Designed by	Checked by	Approved by	Date	Date	
Erlend Røneid				26.06.2020	

	Dynamic calibration		
	Mount electric motor	Edition	Sheet 1 / 1

Appendix C

CRHT-X Paper

Appendix C presents an article made for International symposium on Current Research in Hydraulic Turbines (CRHT-X)

Pressure pulsations at Iveland Power Plant

E Røneid*, B W Solemslie, O G Dahlhaug, J O Kverno

Department of Energy and Process Engineering Norwegian University of Technology and Science, Trondheim, Norway

*Corresponding author (erleron@stud.ntnu.no)

Abstract. Iveland 2 is a power plant located in the south part of Norway that was commissioned in 2016. Since the start up they have been struggling with loud noise and vibrations when the turbine is running at part load. In order to investigate what causes these vibrations, the pressure pulsations will be measured and analysed. To measure the pressure pulsation, two pressure sensors will be placed at the draft tube, and one at the inlet. In addition there will be done test with reduced air flow to the draft tube, to see if that affect the pressure pulsations. The measurement showed that the pressure pulsation were dominated by the Vortex rope. The reduced air flow at the air intake had little effect on the on amplitude. A spectral analysis of an audio recording showed that the frequency of the noise may lie in the range of 60-70 Hz.

1. Introduction

Iveland Power Plant is located in the Aust-Agder in Norway. It was commissioned in 2016 and has struggled with vibrations and loud noise since the start up. The vibration occur when running at part load and is believed to be caused by the flow in the draft tube. The host, Agder Energi, has asked for help to find out what is the problem. The plan is to measure the pressure pulsations in order to find out what causes them. The turbine is equipped with an air intake into the draft tube. There will also be done tests with different flow rates of air to see how that influence the pressure pulsations.

Table 1: General information about Iveland 2 [1]

Characteristic	Data
Commissioned	2016
Head	50m
Turbine	Francis
Rated power	44 MW
BEP	$\sim$ 39 MW
RPM	176,47

2. Pressure pulsations in a Francis Turbine

When the turbine is operating below or above its design point, the water leaving the blade will have a velocity component that moves in the tangential direction, as shown in Figure 1. This creates a swirl in the draft tube because the angle β and rotational speed u is fixed and the flow rate is off the design point. Experiments have shown that swirling flow in a pipe tend to separate the flow in to two regions, where the movement of water mainly happens at the outer region [2] . When the swirl ratio becomes big enough, a stagnation point forms in the inner region.

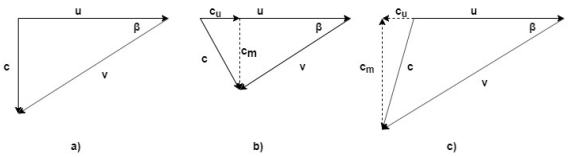

Figure 1: **a)** shows the velocity triangle with the guide vanes at BEP, **b)** shows guide vanes below BEP and **c)** show the guide vanes above BEP

At part load, a helix shaped vortex might appear at the border between the two regions, often referred to as a 'Rotating Vortex Rope'. If the pressure in the draft tube becomes lower than the vapour pressure, the vortex rope becomes visible, as shown in Figure 2. This rope creates a pressure pulsation as it is rotating in the draft tube. The frequency of the pulsation is called the Rheingans frequency, named after W.J. Rheingans, who estimated the relative frequency to be [2]:

$$\frac{f_p}{f_n} \simeq 0.278 \tag{1}$$

where f_p is the frequency at the pressure pulsation created by the vortex rope and f_n is the runner frequency.

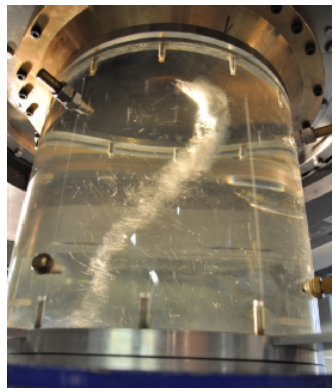

Figure 2: Vortex rope. Photo: Bjørn Winther Solemslie

The vortex rope pulsation consist of two components with the same frequency, an asynchronous and a synchronous component [3]. The synchronous part has equal phase and amplitude in cross section and may be seen as an axisymmetric pressure wave as it propagates through the draft tube. The asynchronous part has a pressure pattern moving around the axis of the draft tube. The components can be calculated using these equations [3]:

$$p_{sync} = \frac{DT1 + DT2}{2} \quad [kPa] \tag{2}$$

$$p_{async} = \frac{DT1 - DT2}{2} \quad [kPa] \tag{3}$$

where $DT1$ and $DT2$ are pressure signals from the same plane but placed 180 degrees apart from each other.

Another source of pressure pulsation can be Von Karman Vortices. These vortices can appear behind a bluff body placed in a fluid with perpendicular flow. The flow will alternate between the sides of the body creating swirls in the wake [2]. This can happen behind the stay vanes, guide vanes and runner blades. If the frequency of the vortex shedding resonates with the natural frequency of the body, it will start to vibrate and may cause cracks and failure of the component.

3. Measurement set up

In order to measure the pressure pulsations, there were placed one pressure sensor at the inlet and two at the draft tube placed opposite of each other. Their placement is shown in figure 3. The plant is also equipped with an air intake that lets air into the draft tube through the shaft. The air is sucked in due to the low pressure in the draft tube hub. The air speed in this pipe were measured in order to estimate how much air was sucked in.

In order to get measurement from the whole operating area, there were taken measurement on eight different operating points from 43 MW to 15 MW listed in Table 2. 23 MW and 43 where measured twice to be able to check repeatability. On 23 MW there were also done measurement with different opening at the air intake to investigate if this will affect the pressure pulsations.

For logging the data a labview program premade at Waterpower laboratory was used. The sample rate was set to 5000 Hz and the logging time was set to 60 seconds. There were done two loggings at each measuring point in case there were some mistake in the reading. Since there were no mistake the logging sequence were added together to improve the frequency resolution. The data was imported in to Matlab and transferred into the frequency domain using Matlabs pwelch function. The hanning window was used as window type with 50 % overlap and the number of windows were eight.

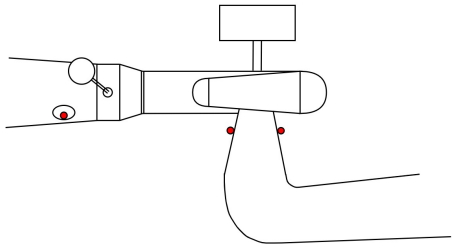

Figure 3: Pressure sensor placement

Table 2: Measuring points

Measurement [#]	Power[MW]	Air intake
1	43	Open
2	39	Open
3	35	Open
4	31	Open
5	27	Open
6	23	Open
7	19	Open
8	15	Open
9	23	Open
10	23	Closed
11	23	Half Closed
12	43	Open

4. Results

The result is presented in Figure 5 and Figure 6. Since the graph from the two sensors are almost identical one sensor is chosen to represent the result. The figures show each measuring point including the ones with varying air flow. The amplitude is normalized with the net head. In Figure 6 the frequency is normalized with the rotational frequency in order to find frequencies that is dependent on the rotational speed. Figure 4 illustrates the difference in pressure pulsations between running on Best Efficiency Point (BEP) at 39 MW and in the problem area at 27 MW.

During the measurement it was observed that the noise started between 31 MW and 27 MW. The noise got significantly worse between 27 MW and 23 MW. During the change in power from 27 MW to 23 MW a video recording was made. There were done a spectral analysis on the audio shown in Figure 7 to determine what frequency that are dominating.

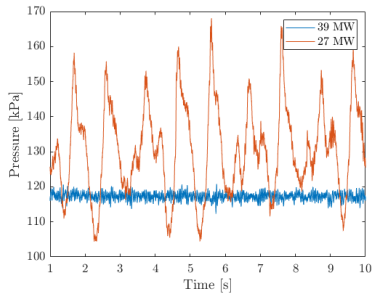

Figure 4: Pressure measurements at 39 and 27 MW in the time domain

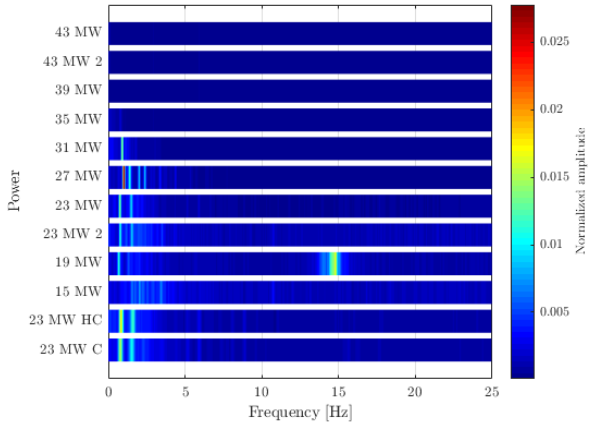

Figure 5: Draft tube sensor 1, showing frequencies from 0 to 25 Hz

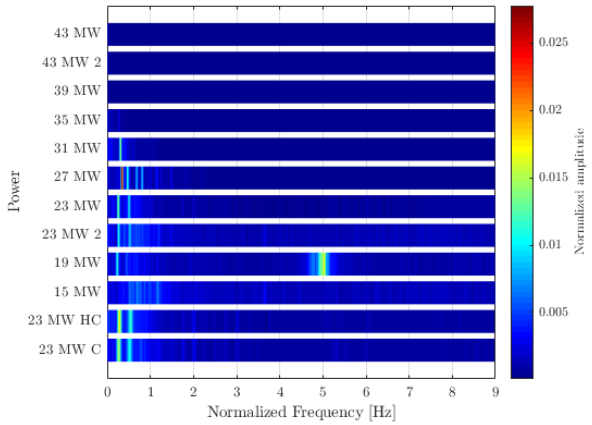

Figure 6: Draft tube sensor 1, with normalized frequencies

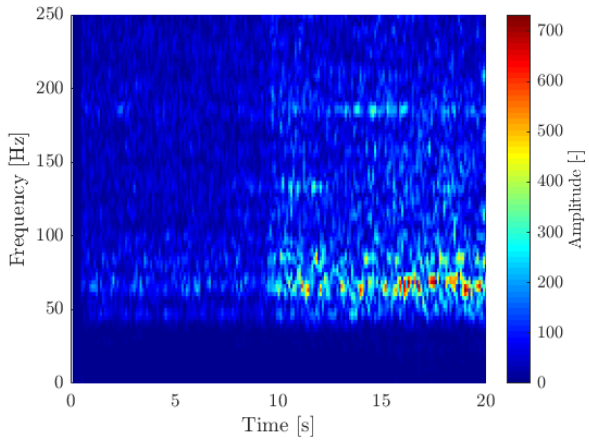

Figure 7: Audio recording of noise when moving from 27MW to 23MW

5. Discussion

Figure 5 show no sign of pressure pulsations at 43 MW and 39 MW. It starts at 35 MW and get worse as the power moves towards 27 MW, before it decreases towards 15 MW. The dominating frequency lies between 0.65 and 0.99. Looking at Figure 6 with the normalized frequency, the dominating frequency lies between 0.33 and 0.22. It matches well with the Rheingans frequency in Equation 1. On both Figure 5 and Figure 6 there can be observed a harmonic after Rheingans frequency.

When running on 23 MW the air flow reduced to see if that would affect the pressure pulsations in any way. 23 MW HC and 23 MW C in Figure 5 show the measurement done with the air intake half closed and closed respectively. There was a small increase in the amplitude when the air flow was reduced.

Since the frequency of the vortex rope is at the most 1 Hz it is suspected that this is not the source of the noise. The audible frequency for humans is 20 Hz and upwards[4]. In figure 7 the change in noise level moving from 27 MW to 23 MW is visible around the ten second mark. It shows a change in amplitude in the range from 60 Hz to 70 Hz. It is possible that this is the source of the loud noise. What phenomena that causes this frequency is not known at the time of writing.

When operating at 19 MW a significant pressure pulsation with a frequency of around 15 Hz appears. The cause of this frequency is not known. Since the frequency is below the audible range for humans, it is believed that this do not contribute to the noise.

6. Further work

In the search for the loud noise the source of the frequency range of 60-70 Hz needs to be investigated further. One possibility that will be pursued is Von Karman Vortices. It difficult to estimate the frequency of vortex shedding but there will done an attempt to see if it can be linked to the stay vanes, guide vanes or the runner blades. Other possibilities apart from Von Karman will also be considered.

The effect of reduced air flow will be looked into in more detail to determine if and how much this effects the pressure pulsations. It could also be interesting to investigate further in the 15 Hz frequency that occurs only at the 19 MW operating point. Another aspect that will be further investigated is the synchronous and asynchronous component of the pressure pulsations.

References

[1] Agder Energi 2018 Iveland kraftverk https://www.ae.no/virksomhet/vannkraft/kraftstasjoner/iveland-kraftstasjon/, Last accessed on 2019-11-04

[2] Dörfler P, Sick M and Coutu A 2013 *Flow-Induced Pulsation and Vibration in Hydroelectric Machinery: Engineer's Guidebook for Planning, Design and Troubleshooting* 2013th ed (London: Springer London) ISBN 978-1-4471-4251-5

[3] Gogstad P J 2017 *Experimental Investigation and Mitigation of Pressure Pulsations in Francis Turbines*

[4] Winther F Ø 2019 *Store medisinske leksikon*

Appendix D

Calibration reports

CALIBRATION REPORT

CALIBRATION PROPERTIES
Calibrated by: Erlend Røneid
Type/Producer: Unik 5000
SN: 3725345
Range: 0-10 bar a
Unit: kPa

CALIBRATION SOURCE PROPERTIES
Type/Producer: Pressurements deadweight tester P3223-1
SN: 66256
Uncertainty [%]: 0,008

POLY FIT EQUATION:
Y= -248.03326060E+0X^0 + 124.92840280E+0X^1

CALIBRATION SUMARY:
Max Uncertainty : 0.003292 [%]
Max Uncertainty : 0.019176 [kPa]
RSQ : 1.000000
Calibration points : 36

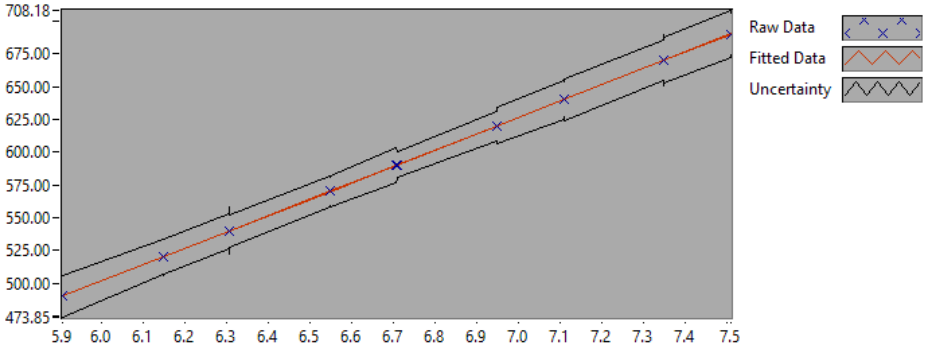

Figure 1 : Calibration chart (The uncertainty band is multiplied by 1000)

Erlend Røneid

CALIBRATION VALUES

Value [kPa]	Voltage [V]	Best Poly Fit [kPa]	Deviation [kPa]	Uncertainty [%]	Uncertainty [kPa]
489.857589	5.906552	489.862848	-0.005260	0.003268	0.016009
519.902910	6.147251	519.932997	-0.030088	0.002659	0.013827
539.933124	6.307371	539.936580	-0.003456	0.003128	0.016888
569.978445	6.547913	569.987059	-0.008614	0.002083	0.011872
590.008659	6.708298	590.023754	-0.015094	0.001890	0.011154
620.053981	6.948949	620.087853	-0.033872	0.002207	0.013682
640.084195	7.109113	640.096857	-0.012663	0.002488	0.015922
670.129516	7.349753	670.159661	-0.030145	0.002861	0.019176
690.159730	7.510136	690.195989	-0.036258	0.002606	0.017988
690.179730	7.510190	690.202722	-0.022992	0.002359	0.016281
670.149516	7.349822	670.168321	-0.018805	0.002575	0.017259
640.104195	7.109159	640.102584	0.001611	0.002521	0.016134
620.073981	6.948881	620.079330	-0.005349	0.002072	0.012846
590.028659	6.708398	590.036247	-0.007588	0.001647	0.009720
569.998445	6.548011	569.999335	-0.000890	0.002142	0.012210
539.953124	6.307553	539.959309	-0.006185	0.002264	0.012226
519.922910	6.147434	519.955875	-0.032965	0.002574	0.013383
489.877589	5.906807	489.894691	-0.017102	0.003254	0.015940
489.877589	5.906715	489.883197	-0.005608	0.003207	0.015709
519.922910	6.147388	519.950071	-0.027161	0.002635	0.013702
539.953124	6.307489	539.951300	0.001824	0.003292	0.017774
569.998445	6.547987	569.996314	0.002132	0.001973	0.011248
590.028659	6.708393	590.035552	-0.006892	0.001954	0.011529
620.073981	6.948885	620.079906	-0.005925	0.001870	0.011595
640.104195	7.109022	640.085493	0.018702	0.002097	0.013422
670.149516	7.349499	670.127958	0.021559	0.002330	0.015612
690.179730	7.509891	690.165461	0.014269	0.002398	0.016548
690.169730	7.509839	690.158935	0.010796	0.002576	0.017778
670.139516	7.349371	670.111934	0.027582	0.002239	0.015008
640.094195	7.108929	640.073853	0.020342	0.002287	0.014636
620.063981	6.948485	620.029915	0.034066	0.001843	0.011428
590.018659	6.707914	589.975751	0.042909	0.002238	0.013207
569.988445	6.547552	569.941955	0.046490	0.002011	0.011460
539.943124	6.307051	539.896572	0.046552	0.002478	0.013380
519.912910	6.146992	519.900605	0.012305	0.002543	0.013223
489.867589	5.906336	489.835814	0.031775	0.003233	0.015838

COMMENTS:

The uncertainty is calculated with 95% confidence. The uncertainty includes the randomness in the calibrated instrument during the calibration, systematic uncertainty in the instrument or property which the instrument under calibration is compared with (dead weight manometer, calibrated weights etc.), and due to regression analysis to fit the calibration points to a linear calibration equation.The calculated uncertainty can be used as the total systematic uncertianty of the calibrated instrument with the given calibration equation.

CALIBRATION REPORT

CALIBRATION PROPERTIES
Calibrated by: Erlend Røneid
Type/Producer: UNIK 5000
SN: 5463597
Range: 0-3 bar a
Unit: kPa

CALIBRATION SOURCE PROPERTIES
Type/Producer: Pressurements deadweight tester P3223-1
SN: 66256
Uncertainty [%]: 0,008

POLY FIT EQUATION:
Y= -74.66128917E+0X^0 + 37.49121989E+0X^1

CALIBRATION SUMARY:
Max Uncertainty : 0.059246 [%]
Max Uncertainty : 0.018410 [kPa]
RSQ : 1.000000
Calibration points : 28

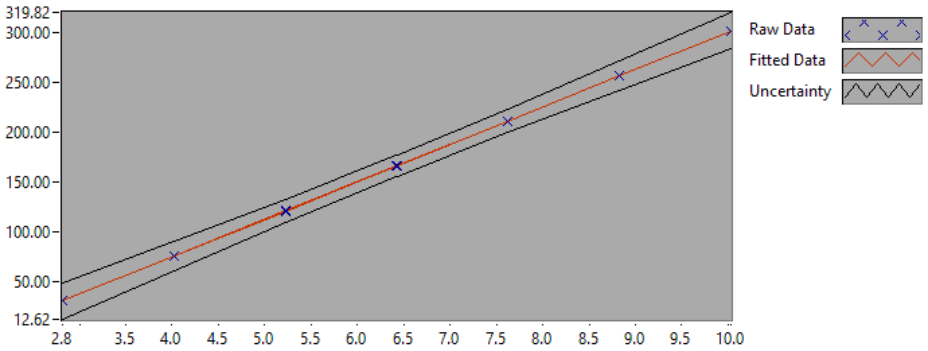

Figure 1 : Calibration chart (The uncertainty band is multiplied by 1000)

Erlend Røneid

CALIBRATION VALUES

Value [kPa]	Voltage [V]	Best Poly Fit [kPa]	Deviation [kPa]	Uncertainty [%]	Uncertainty [kPa]
30.994250	2.818516	31.008298	-0.014047	0.059148	0.018332
76.062232	4.020622	76.076743	-0.014510	0.018923	0.014393
121.110214	5.222431	121.134030	-0.023816	0.009409	0.011396
166.178196	6.424394	166.197082	-0.018886	0.006155	0.010228
211.216178	7.626579	211.268465	-0.052287	0.005441	0.011493
256.304160	8.829467	256.366182	-0.062022	0.005651	0.014483
301.372142	10.031304	301.424550	-0.052408	0.006105	0.018399
301.402142	10.030395	301.390473	0.011669	0.006092	0.018362
256.334160	8.828521	256.330733	0.003427	0.005633	0.014439
211.266178	7.626329	211.259071	0.007107	0.005407	0.011424
166.208196	6.423857	166.176953	0.031243	0.006143	0.010211
121.140214	5.221943	121.115728	0.024486	0.009408	0.011397
76.072232	4.020109	76.057493	0.014739	0.018916	0.014390
31.004250	2.818148	30.994515	0.009735	0.059129	0.018332
31.024250	2.819920	31.060958	-0.036708	0.059094	0.018334
76.072232	4.020731	76.080805	-0.008573	0.018934	0.014404
121.140214	5.222448	121.134642	0.005572	0.009443	0.011439
166.208196	6.424463	166.199671	0.008525	0.006165	0.010247
211.266178	7.626651	211.271169	-0.004991	0.005403	0.011414
256.314160	8.828100	256.314967	-0.000807	0.005647	0.014474
301.372142	10.029613	301.361151	0.010991	0.006109	0.018410
301.372142	10.029196	301.345487	0.026655	0.006106	0.018402
256.294160	8.826775	256.265292	0.028868	0.005692	0.014588
211.216178	7.624460	211.189017	0.027161	0.005410	0.011427
166.148196	6.422039	166.108769	0.039427	0.006158	0.010231
121.080214	5.220198	121.050297	0.029918	0.009448	0.011440
76.022232	4.018666	76.003414	0.018818	0.018989	0.014436
30.954250	2.817322	30.963536	-0.009286	0.059246	0.018339

COMMENTS:

The uncertainty is calculated with 95% confidence. The uncertainty includes the randomness in the calibrated instrument during the calibration, systematic uncertainty in the instrument or property which the instrument under calibration is compared with (dead weight manometer, calibrated weights etc.), and due to regression analysis to fit the calibration points to a linear calibration equation.The calculated uncertainty can be used as the total systematic uncertianty of the calibrated instrument with the given calibration equation.

CALIBRATION REPORT

CALIBRATION PROPERTIES
Calibrated by: Erlend Røneid
Type/Producer: UNIK 5000
SN: 5472337
Range: 0-3 bar a
Unit: kPa

CALIBRATION SOURCE PROPERTIES
Type/Producer: Pressurements deadweight tester P3223-1
SN: 66256
Uncertainty [%]: 0,008

POLY FIT EQUATION:
Y= -74.66743977E+0X^0 + 37.48787199E+0X^1

CALIBRATION SUMARY:
Max Uncertainty : 0.042394 [%]
Max Uncertainty : 0.013224 [kPa]
RSQ : 1.000000
Calibration points : 28

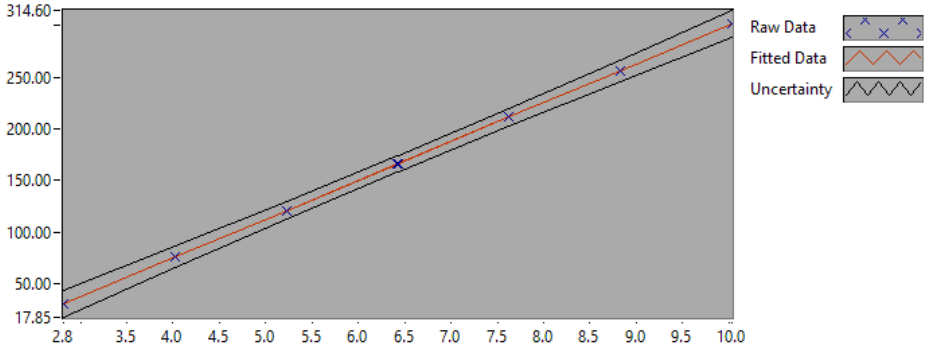

Figure 1 : Calibration chart (The uncertainty band is multiplied by 1000)

Erlend Røneid

CALIBRATION VALUES

Value [kPa]	Voltage [V]	Best Poly Fit [kPa]	Deviation [kPa]	Uncertainty [%]	Uncertainty [kPa]
30.994250	2.818717	31.000269	-0.006018	0.042319	0.013117
76.062232	4.020878	76.066713	-0.004481	0.013548	0.010305
121.110214	5.222673	121.119453	-0.009239	0.006745	0.008169
166.178196	6.424442	166.171225	0.006971	0.004423	0.007350
211.216178	7.626805	211.245239	-0.029061	0.003916	0.008272
256.304160	8.829690	256.338850	-0.034690	0.004067	0.010423
301.372142	10.031721	301.400424	-0.028282	0.004377	0.013191
301.402142	10.031342	301.386227	0.015915	0.004363	0.013151
256.334160	8.829648	256.337292	-0.003132	0.004044	0.010367
211.266178	7.627321	211.264580	0.001598	0.003883	0.008204
166.208196	6.424725	166.181829	0.026367	0.004409	0.007328
121.140214	5.222599	121.116674	0.023540	0.006743	0.008168
76.072232	4.020726	76.061029	0.011203	0.013538	0.010299
31.004250	2.818644	30.997524	0.006726	0.042304	0.013116
31.024250	2.820511	31.067517	-0.043267	0.042285	0.013119
76.072232	4.021462	76.088617	-0.016385	0.013560	0.010315
121.140214	5.223124	121.136362	0.003852	0.006781	0.008215
166.208196	6.425219	166.200337	0.007859	0.004443	0.007385
211.266178	7.627433	211.268785	-0.002607	0.003880	0.008196
256.314160	8.829324	256.325143	-0.010984	0.004071	0.010435
301.372142	10.031097	301.377022	-0.004880	0.004388	0.013224
301.372142	10.030922	301.370498	0.001644	0.004379	0.013198
256.294160	8.828187	256.282516	0.011644	0.004102	0.010513
211.216178	7.625466	211.195052	0.021126	0.003887	0.008211
166.148196	6.422951	166.115339	0.032857	0.004426	0.007354
121.080214	5.220941	121.054547	0.025668	0.006789	0.008220
76.022232	4.019283	76.006921	0.015311	0.013619	0.010354
30.954250	2.818003	30.973507	-0.019257	0.042394	0.013123

COMMENTS:

The uncertainty is calculated with 95% confidence. The uncertainty includes the randomness in the calibrated instrument during the calibration, systematic uncertainty in the instrument or property which the instrument under calibration is compared with (dead weight manometer, calibrated weights etc.), and due to regression analysis to fit the calibration points to a linear calibration equation.The calculated uncertainty can be used as the total systematic uncertianty of the calibrated instrument with the given calibration equation.

Appendix E

Documentation for pressure sensors

GE
Measurement & Control

UNIK 5000

Pressure Sensing Platform

The new UNIK 5000 is a high performance configurable solution to pressure measurement. The use of micromachined silicon technology and analogue circuitry enables best in class performance for stability, low power and frequency response. The new platform enables you to easily build up your own sensor to match your own precise needs. This high performance, configurable solution to pressure measurement employs modular design and lean manufacturing techniques to offer:

High Quality

The combination of a high technology sensor, together with advanced signal conditioning and packaging techniques, provides an ideal long term solution for reliable, accurate and economical measurements

Bespoke as Standard

Custom-built from standard components, manufacturing sensors to your requirement is fast and simple; each UNIK 5000 is a "bespoke" pressure sensing solution, but with the short lead times and competitive pricing you would expect from standard products.

Expertise

We have the people and the knowledge to support your needs for accurate and reliable product performance; our team of experts can help you make the right sensor selection, guiding you and providing the help and tools you need. It is important to ensure that the sensor material and performance selected are suitable for your application.

GE imagination at work

Features

- Ranges from 70 mbar (1 psi) to 700 bar (10000 psi)
- Accuracy to ±0.04% Full Scale (FS) Best Straight Line (BSL)
- Stainless Steel construction
- Frequency response to 3.5 kHz
- High over pressure capability
- Hazardous Area certifications
- mV, mA, voltage and configurable voltage outputs
- Multiple electrical & pressure connector options
- Operating temperature ranges from –55 to 125°C (-67 to 257°F)

5000 Specifications

Measurement

Operating Pressure Ranges

Gauge ranges

Any zero based range 70 mbar to 70 bar
(1 to 1000 psi) (values in psi are approximate)

Sealed Gauge Ranges

Any zero based range 10 to 700 bar
(145 to 10000 psi)

Absolute Ranges

Any zero based range 100 mbar to 700 bar
(1.5 to 10000 psi)

Differential Ranges

Wet/Dry

Uni-directional or bi-directional 70 mbar to 35 bar
(1 to 500 psi)

Wet/Wet

Uni-directional or bi-directional 350 mbar to 35 bar
(5 to 500 psi)

Line pressure: 70 bar max (1000 psi)

Barometric Ranges

Barometric ranges are available with a minimum span of 350 mbar (5.1 psi)

Non Zero Based Ranges

Non zero based ranges are available. For non zero based gauge ranges, please contact GE Measurement & Control to discuss your requirements.

Over Pressure

- 10 × FS for ranges up to 150 mbar (2 psi)
- 6 × FS for ranges up to 700 mbar (10 psi)
- 2 × FS for barometric ranges
- 4 × FS for all other ranges (up to 200 bar for ranges ≤70 bar and up to 1200 bar for ranges >70 bar)

For differential versions the negative side must not exceed the positive side by more than:

- 6 × FS for ranges up to 150 mbar (2 psi)
- 4 × FS for ranges up to 700 mbar (10 psi)
- 2 × FS for all other ranges up to a maximum of 15 bar (200 psi)

Containment Pressure

Ranges up to 150 mbar (2 psi) gauge 10 x FS
Ranges up to 70 bar (1000 psi) gauge 6 x FS
(200 bar (2900 psi) max)
Ranges up to 70 bar (1000 psi) absolute
200 bar (2900 psi)
Ranges above 70 bar (1000 psi)
1200 bar (17400 psi)

Differential (-ve port) must not exceed positive port by more than 6 × FS (15 bar (200 psi) maximum)

Supply and Outputs

Electronics Option	Description	Supply voltage (V)	Output	Current Consumption (mA)
0	mV Passive	2.5 to 12	10 mV/V^	<2 at 10 V
1	mV Linearised	7 to 12	10 mV/V^	<3
2	mA	7 to 28**	4-20 mA	<30
3	0 to 5 V 4-wire	7 to 16**	0 to 5 V	<3
4	0 to 5 V 3-wire	7 to 16**	0 to 5 V*	<3
5	Basic Configurable (3-wire)	See below~	See below	<3
6	0 to 10 V 4-wire	12 to 16**	0 to 10 V	<3
7	0.5 V to 4.5 V Ratiometric	5.0 ± 0.5	0.5 to 4.5 V	<3
8	Configurable (4-wire)	7 to 36	See below	See below
9	Configurable (3-wire)	7 to 36	See below	See below

^ with a 10 V supply mV output sensors give 100 mV over the full scale pressure.
• Output is ratiometric to the supply voltage
• Output reduces pro-rata for pressure ranges below 350 mbar (5 psi)
**0 to 5 V 3-wire output is non true zero. At pressures below 1% of span the output will be fixed at approximately 50 mV*
***32 V in non-hazardous area operation*
~ Supply voltage is between [Maximum Output + 1 V] (7 V minimum) to 16 V (32 V in non-hazardous area operation)

Basic Configurable (Option 5), Configurable 4-Wire (Option 8), Configurable 3-Wire (Option 9)

Any pressure signal output configurations will be available, subject to the following limitations:

Output specification	Basic Configurable (Option 5)	Configurable (Options 8, 9)
Minimum span:	4 V	2 V
Maximum span:	10 V	20 V
Maximum output limit:	11 V	±10 V
Maximum zero offset:	Span / 2	±Span
Current consumption:	< 3 mA	< 20 mA @ 7 Vdc decreasing to < 5 mA @ 32 Vdc
Reverse output response:	No	Yes
Maximum operating temperature:	+125˚C	+80˚C

Output voltage range can be specified to a resolution of 0.1 V.
The output will continue to respond to 110% FS. i.e. if a 0 to 10 V output is specified, the output will continue to increase proportionally to applied pressure until at least 11 V.
Option 5: Not true zero, the output will saturate at < 50 mV.
Options 8, 9: On startup <100 mA drawn for 10 ms typically.
Options 8, 9: Shunt calibration: not available with reverse output.

Examples

Configuration	Allowed	Not Allowed
Basic Configurable (Option 5)	0 to 5 V	1 to 4 V (span too small)
	0.5 to 4.5 V	4 to 11 V (offset too big)
	1 to 6 V	
	1 to 11 V	
Configurable (Options 8, 9)	-10 to 0 V	0 to 12 V (outside ±10 V limits)
	0 to 5 V	6 to 10 V (offset too big)
	-5 to 5 V	0 to 0.5 V (span too small)
	-2 to 10 V	
	1 to 6 V	
	10 to 0 V	

Power-Up Time
- mV, Voltage and current versions: 10 ms
- Configurable 3-wire and 4-wire versions: 500 ms

Insulation
- 500 Vdc: 100 MΩ
- 500 Vac: ≤ 5 mA leakage current (mV and mA versions only).

Shunt Calibration
Shunt Calibration provides a customer accessible connection which, when applied, causes a shift in output of 80% FS in order to simulate applied pressure.
It is fitted to the mV, Configurable 4-wire and Configurable 3-wire versions as standard. It is not available with DIN, M12 x 1 or M20 x 1.5 electrical connectors (options 7, D, G and R)

Shunt calibration is activated in different ways depending on the electrical connector and version:
- mV versions: connect Shunt Cal to -ve Supply or, where available, connect both Shunt Cal connections together.
- Configurable 4-wire and Configurable 3-wire versions: connect Shunt Cal to -ve Output or, where available, connect both Shunt Cal connections together.

Note: Not available with reverse output.

Performance Specifications

There are three grades of performance specification: Industrial, Improved and Premium.

Accuracy
Voltage, Current and mV Linearised
Combined effects of non-linearity, hysteresis and repeatability:

Industrial:	±0.2% FS BSL
Improved:	±0.1% FS BSL
Premium:	±0.04% FS BSL

mV Passive
≤ 70 bar

Industrial/Improved:	±0.25% FS BSL
Premium not available	

> 70 bar

Industrial/Improved:	±0.5% FS BSL
Premium not available	

Note: For the barometric pressure range, accuracy is of span, not full scale.

Zero Offset and Span Setting
Demountable electrical connector options allow access to potentiometers that give at least ±5% FS adjustment (see Electrical Connector section)

Factory set to:

Product Description	Industrial	Improved and Premium
Current and Voltage Versions (Demountable Electrical Connections and Cable Gland)	±0.5% FS	±0.2% FS
Current and Voltage Versions (All Other Electrical Connections)	±1.0% FS	±1.0% FS
mV Versions	±3.0 mV	±3.0 mV

Long Term Stability
±0.05% FS typical (±0.1% FS maximum) per year increasing pro-rata for pressure ranges below 350 mbar

Temperature Effects
Four compensated temperature ranges can be chosen.
Industrial Accuracy performance:

-10 to +50°C (14 to +122°F):	±0.75% FS Temperature error band (TEB)
-20 to +80°C (-4 to +176°F):	±1.5% FS TEB
-40 to +80 °C (-40 to +176°F):	±2.25% FS TEB
-40 to +125°C (-40 to +257°F):	±2.25% FS TEB

Improved and Premium Accuracy performance:

-10 to +50°C (14 to +122°F):	±0.5% FS TEB
-20 to +80°C (-4 to +176°F):	±1.0% FS TEB
-40 to +80°C (-40 to +176°F):	±1.5% FS TEB
-40 to +125°C (-40 to +257°F):	±1.5% FS TEB

Temperature effects increase pro-rata for pressure ranges below 350 mbar (5 psi) and are doubled for barometric ranges.

Line Pressure Effects (Differential Version Only)
Zero shift: <±0.03% span/bar of line pressure
Span shift: <±0.03% span/bar of line pressure
Effects increase pro-rata for differential pressure ranges below 700 mbar (10 psi).

Physical Specifications

Environmental Protection
- See Electrical Connector section
- Hyperbaric Pressure: 20 bar (300 psi) maximum

Operating Temperature Range
See Electrical Connector section

Pressure Media
Fluids compatible with stainless steel 316L and Hastelloy C276.
For the wet/dry differential version, negative pressure port: fluids compatible with stainless steel 316L, stainless steel 304, Pyrex, silicon and structural adhesive.

Enclosure Materials

Stainless steel (body), nitrile- or silicone-rubber (o-rings, gaskets), EPDM (gaskets), PVDF (depth cone), PTFE (vent filter), Nickel plated brass (lock rings), glass filled nylon (electrical connector assemblies), delrin (depth cone). Cable sheaths as specified (see Electrical Connector).

Pressure Connector

Available options are

- G1/4 Female*
- G1/4 Male Flat
- G1/4 Male 60° Internal Cone
- G1/4 Male Flat Long
- G1/4 Male Flat with Snubber
- G1/4 Male Flat with Cross Bore Protection
- G1/4 Male with Nipple
- G1/4 Quick Connect
- G1/8 Male 60° Internal Cone
- G1/2 Male via Adaptor*
- 1/4 NPT Female*
- 1/4 NPT Male
- 1/8 NPT Male
- 1/2 NPT Male via Adaptor
- 7/16-20 UNF Female
- 7/16-20 UNF Male Short Flat
- 7/16 UNF Long 37° Flare Tip
- 7/16-20 UNJF Male 74° External Cone
- 3/8-24 UNJF
- 1/4 Swagelok Bulkhead
- M10 X 1 80° Internal Cone
- M12 X 1 60° Internal Cone
- M14 X 1.5 60° Internal Cone
- M20 X 1.5 Male
- Depth Cone (G1/4 Female Open Face)
- M12 x 1.0 74° External Cone
- Quick Release Male
- VCR Female*
- VCR Male*
- NW16 Flange
- R3/8 Male
- R1/4 Male

Choose connectors marked * for pressure ranges over 70 bar. Other pressure connectors may be available, contact GE to discuss your requirement.

General Certifications

RoHS 2002/95/EC
CRN Certified 0F13650.517890YTN ADD1/ REV1, 0F13828.2 (sensor types K and O) and CSA 0F13650.56 ADD1 for pressure ranges up to and including 350 bar (5000 psi)

Electrical Connector

Various electrical connector options are available offering different features:

Code Number	Description	Max Operating temp range		IP rating	Zero span Adjust
		°C	°F		
0	No Connector	-55 to +125	-67 to +257	-	Y
1	Cable Gland	-40 to +80	-40 to +176	65	N
2	Raychem Cable	-55 to +125	-67 to +257	65	N
3	Polyurethane Depth	-40 to +80	-40 to +176	68	N
4	Hytrel Depth	-40 to +80	-40 to +176	68	N
6/E	Bayonet MIL-C-26482	-55 to +125	-67 to +257	67	N
7	DIN 43650 Form A Demountable	-40 to +80	-40 to +176	65	Y
A/F	Bayonet MIL-C-26482 Demountable	-55 to +125	-67 to +257	65	Y
C	1/2 NPT Conduit	-40 to +80	-40 to +176	65	N
D	Micro DIN (9.4 mm pitch)	-40 to +80	-40 to +176	65	N
G	M12x1 4pin	-55 to +125	-67 to +257	67	N
K	Zero Halogen Cable Demountable	-40 to +80	-40 to +176	65	Y
M	Tajimi R03-R6F	-25 to +85	-13 to +185	65	N
R	M20 x 1.5 Inline	-40 to +80	-40 to +176	65	Y

Note: Electronics output options 8 and 9 are restricted to a maximum operating temperature of 80°C (176°F).
Note: Hazardous area approved versions are restricted to a maximum operating temperature range of -40°C to 80°C (-40°F to 176°F).
Note: Electrical connector option R IP65 rating only with suitable conduit/cable fitting.

CE Conformity

Pressure Equipment Directive 97/23/EC: Sound Engineering Practice
ATEX 94/9/EC (Optional)
EMC Directive 2004/108/EC

BS EN 61000-6-1: 2007	Susceptibility - Light Industrial
BS EN 61000-6-2: 2005	Susceptibility - Heavy Industrial (except mV versions)
BS EN 61000-6-3: 2007	Emissions - Light Industrial
BS EN 61000-6-4: 2007	Emissions - Heavy Industrial
BS EN 61326-1: 2006	Electrical Equipment for Measurement, Control and Laboratory Use
BS EN 61326-2-3: 2006	Particular Requirements for Pressure Transducers

Hazardous Area Approvals (optional)

General applications
- IECEx/ATEX Intrinsically Safe 'ia' Group IIC
- INMETRO Intrinsically Safe 'ia' Group IIC
- NEPSI Intrinsically Safe 'ia' Group IIC
- FM Approved (Canada & US) Intrinsically Safe Exia Class I, Division 1, Groups A, B, C & D and Class I, Zone 0 AEx/Ex ia Group IIC; Single Seal

Mining applications
- IECEx/ATEX Intrinsically Safe 'ia' Group I
- INMETRO Intrinsically Safe 'ia' Group I

For full certification details, refer to the type-examination certificates (or approval listings) and supplied hazardous area installation instructions.

Electrical Connector

Connector Type	Option code		Electronics Option					
			4 to 20 mA	Voltage (3-wire) and Basic Configurable	Voltage (4-wire)	Configurable Voltage (4-Wire)	Configurable Voltage (3-Wire)	mV
Molex	0	1 Red	+ve Supply	+ve Supply	+ve Supply	+ve Supply	+ve Supply	+ve Supply
		2 Yellow	-	+ve Output	+ve Output	+ve Output	+ve Output	+ve Output
		3 Green	-	-	-ve Output	-ve Output	0V Common	-ve Output
		4 Blue	-ve Supply	0V Common	-ve Supply	-ve Supply	0V Common	-ve Supply
		5 Orange	-	-	-	Shunt Cal	Shunt Cal	Shunt Cal
		6 Black	Case	Case	Case	Case	Case	-
Cable (Not Raychem)	1, 3, 4, C	Red	+ve Supply	+ve Supply	+ve Supply	+ve Supply	+ve Supply	+ve Supply
		Yellow	-	+ve Output	+ve Output	+ve Output	+ve Output	+ve Output
		Blue	-	-	-ve Output	-ve Output	0V Common	-ve Output
		White	-ve Supply	0V Common	-ve Supply	-ve Supply	0V Common	-ve Supply
		Orange	-	-	-	Shunt Cal	Shunt Cal	Shunt Cal
		Black	-	-	-	-	-	-
		Screen	-	-	-	-	-	-
Raychem Cable	2	Red	+ve Supply	+ve Supply	+ve Supply	+ve Supply	+ve Supply	+ve Supply
		White	-	+ve Output	+ve Output	+ve Output	+ve Output	+ve Output
		Green	-	-	-ve Output	-ve Output	0V Common	-ve Output
		Blue	-ve Supply	0V Common	-ve Supply	-ve Supply	0V Common	-ve Supply
		Black	-	-	-	Shunt Cal	Shunt Cal	Shunt Cal
		Screen	-	-	-	-	-	-
Bayonet	6, A	A	+ve Supply	+ve Supply	+ve Supply	+ve Supply	+ve Supply	+ve Supply
		B	-ve Supply	+ve Output	+ve Output	+ve Output	+ve Output	+ve Output
		C	-	-	-ve Output	-ve Output	0V Common	-ve Output
		D	-	0V Common	-ve Supply	-ve Supply	0V Common	-ve Supply
		E	-	-	-	Shunt Cal	Shunt Cal	Shunt Cal
		F	-	-	-	-	-	Shunt Cal
DIN A Micro DIN	7 D	1	+ve Supply	+ve Supply	+ve Supply	+ve Supply	+ve Supply	+ve Supply
		2	-ve Supply	0V Common	-ve Supply	-ve Supply	0V Common	-ve Supply
		3	-	+ve Output	+ve Output	+ve Output	+ve Output	+ve Output
		E	Case	Case	-ve Output	-ve Output	0V Common	-ve Output
Bayonet Alternative Wiring Options	E, F	A	+ve Supply	+ve Supply	+ve Supply	+ve Supply	+ve Supply	+ve Supply
		B	-	0V Common	-ve Supply	-ve Supply	0V Common	-ve Supply
		C	-	+ve Output	+ve Output	+ve Output	+ve Output	+ve Output
		D	-ve Supply	-	-ve Output	-ve Output	0V Common	-ve Output
		E	-	-	-	Shunt Cal	Shunt Cal	Shunt Cal
		F	-	-	-	Shunt Cal	Shunt Cal	-
M12 X 1 4-Pin	G	1	+ve Supply	+ve Supply	+ve Supply	+ve Supply	+ve Supply	+ve Supply
		2		+ve Output	+ve Output	+ve Output	+ve Output	+ve Output
		3	-ve Supply	0V Common	-ve Supply	-ve Supply	0V Common	-ve Supply
		4	Case	Case	-ve Output	-ve Output	0V Common	-ve Output
Zero Halogen Cable (Demountable)	K	Pink	+ve Supply	+ve Supply	+ve Supply	+ve Supply	+ve Supply	+ve Supply
		White	-	+ve Output	+ve Output	+ve Output	+ve Output	+ve Output
		Green	-	-	-ve Output	-ve Output	0V Common	-ve Output
		Blue	-ve Supply	0V Common	-ve Supply	-ve Supply	0V Common	-ve Supply
		Grey	-	-	-	Shunt Cal	Shunt Cal	Shunt Cal
		Brown	-	-	-	-	-	-
		Yellow	-	-	-	-	-	-
		Screen	-	-	-	-	-	-
Tajimi R03-R6F	M	A	+ve Supply	+ve Supply	+ve Supply	+ve Supply	+ve Supply	+ve Supply
		B	-	0V Common	-ve Supply	-ve Supply	0V Common	-ve Supply
		C	-ve Supply	Case	Case	Case	Case	-
		D	-	-	-ve Output	-ve Output	0V Common	-ve Output
		E	Case	+ve Output	+ve Output	+ve Output	+ve Output	+ve Output
		F	-	-	Shunt cal	Shunt cal	Shunt Cal	Shunt cal
M20 x 1.5 Female Demountable	R	+ve	+ve Supply	-	-	-	-	-
		-ve	-ve Supply	-	-	-	-	-

Ordering Information

See the online configuration tool at www.unik5000.com

(1) Select model number

Main Product Variant

PMP Amplified Pressure Transducer
PDCR mV Pressure Transducer
PTX 4-20 mA Pressure Transmitter

Product Series
5 UNIK 5000

Diameter and Material
0 25mm Stainless Steel

Electrical Connector Note 6
0 No Electrical Connector **Note 7**
1 Cable Gland (Polyurethane Cable)
2 Raychem Cable
3 Polyurethane Cable (Depth)
4 Hytrel Cable (Depth)
6 MIL-C-26482 (6-pin Shell Size 10) (Mating connector not supplied)
7 DIN 43650 Form A Demountable (Mating connector supplied)
A Demountable MIL-C-26482 (6-pin Shell Size 10) (Mating connector not supplied)
C 1/2" NPT Conduit (Polyurethane cable)
D Micro DIN (9.4 mm Pitch) (Mating connector supplied)
E MIL-C-26482 (6 pin Shell Size 10) Alternative Wiring (Mating connector not supplied)
F Demountable MIL-C-26482 (6 pin Shell Size 10) Alternative Wiring (Mating connector not supplied)
G M12 x 1 4-pin male (Mating connector not supplied)
K Zero Halogen Cable Demountable
M Tajimi R03-R6F
R M20 x 1.5 Inline Female Conduit Demountable **Note 8**

Electronics Option
0 mV Passive 4-wire (PDCR) **Note 1**
1 mV Linearised 4-wire (PDCR)
2 4 to 20 mA 2-wire (PTX)
3 0 to 5 V 4-wire (PMP)
4 0 to 5 V 3-wire (PMP)
5 Basic Configurable 3-wire (PMP)
6 0 to 10 V 4-wire (PMP)
7 0.5 to 4.5 V Ratiometric 3-wire (PMP) **Note 5**
8 Configurable 4-wire (PMP) **Note 4, 5**
9 Configurable 3-wire (PMP) **Note 4, 5**

Compensated Temperature Range
TA -10 to +50 °C (14 to +122 °F)
TB -20 to +80 °C (-4 to +176 °F)
TC -40 to +80 °C (-40 to +176 °F)
TD -40 to +125 °C (-40 to +257 °F) **Note 2, 5**

Accuracy
A1 Industrial
A2 Improved
A3 Premium

Calibration
CA Zero/Span Data
CB Room Temperature
CC Full Thermal

Hazardous Area Approval Note 6
H0 None
H1 IECEx/ATEX Intrinsically Safe 'ia' Group IIC
H2 IECEx/ATEX Intrinsically Safe 'ia' Group I
H6 FM (C & US) Intrinsically Safe 'ia' Group IIC/ABCD
HA IECEx/ATEX Intrinsically Safe 'ia' Groups I/IIC [H1 + H2]
HS IECEx/ATEX/FM (C & US) Intrinsically Safe 'ia' Groups IIC/ABCD [H1 + H6]
J1 IECEx/ATEX/NEPSI Intrinsically Safe 'ia' Group IIC
JA INMETRO Intrinsically Safe 'ia' Group IIC
JB INMETRO Intrinsically Safe 'ia' Group I
JF INMETRO Intrinsically Safe 'ia' Group I/IIC [JA + JB]

Pressure Connector

PA	G1/4 Female **Note 3**	**PV**	7/16-20 UNF Female
PB	G1/4 Male Flat	**PW**	Depth Cone (G1/4 Female Open Face)
PC	G1/4 Male 60° Internal Cone	**PX**	7/16-20 UNF Male Short Flat
PD	G1/8 Male 60° Internal Cone	**PY**	3/8-24 UNJF
PE	1/4 NPT Female **Note 3**	**PZ**	M10 x 1 80° Internal Cone
PF	1/4 NPT Male	**RA**	VCR Female **Note 3, 9**
PG	1/8 NPT Male	**RB**	G1/4 Male Flat with Snubber
PH	M20x1.5	**RC**	G1/4 Male Flat with Cross Bore Protection
PJ	M14x1.5 60° Internal Cone	**RD**	M12 x 1.0 74° External Cone
PK	M12x1 Internal Cone	**RE**	Quick Release Mount
PL	7/16-20 UNJF Male 74° External Cone	**RF**	VCR Male **Note 3, 9**
PN	G1/2 Male via Adaptor **Note 3**	**RQ**	NW16 Flange
PQ	G1/4 Quick Connect	**RU**	R3/8 Male
PR	1/2 NPT Male via Adaptor **Note 3**	**RV**	R1/4 Male
PS	1/4 Swagelok Bulkhead	**RW**	G1/4 Male with Nipple
PT	G1/4 Male Flat Long		
PU	7/16-20 UNF Long 37° Flare Tip		

PTX	**5**	**0**	**7**	**2**	**-**	**TA**	**-**	**A2**	**-**	**CB**	**-**	**H0**	**-**	**PA**

Typical Model Number

Ordering Notes

Note 1 Premium Accuracy is not available on this version
Note 2 Please ensure that the electrical connector selected is option 0, 2, 6, A, E, F or G.
Note 3 Select one of these pressure connectors for pressure ranges over 70 bar
Note 4 Max operating temperature is 80°C (176°F)
Note 5 Hazardous area certifications not available
Note 6 Hazardous area certifications are restricted by electrical connector options in line with the following table:

	Connector													
Approval	0	1	2	3	4	6/E	7	A/F	C	D	G	K	M	R
H0	Y	Y	Y	Y	Y	Y	Y	Y	Y	Y	Y	Y	Y	Y
H1	Y	Y	Y	Y	Y	Y	Y	Y	Y	Y	Y	-	-	Y
H2	Y	-	Y	Y	Y	Y	-	-	Y	-	Y	-	-	-
H6	Y	Y	Y	Y	Y	Y	Y	Y	Y	Y	Y	-	-	-
HA	Y	-	Y	Y	Y	Y	-	-	Y	-	Y	-	-	-
HS	Y	Y	Y	Y	Y	Y	Y	Y	Y	Y	Y	-	-	-
J1	Y	Y	Y	Y	Y	Y	Y	Y	Y	Y	Y	-	-	Y
JA	Y	Y	Y	Y	Y	Y	Y	Y	Y	Y	Y	-	-	Y
JB	Y	-	Y	Y	Y	Y	-	-	Y	-	Y	-	-	-
JF	Y	-	Y	Y	Y	Y	-	-	Y	-	Y	-	-	-

Note 7 Available with component certification, use of which requires incorporation into certified apparatus with an IP rated enclosure appropriate to the certification type supplied.
Note 8 Electronics option 2 only.
Note 9 Pressure ranges less than 500 bar.

2) State pressure range and units: e.g. 0 to 10 bar, -5 to + 5 psi

Unit options are:

Symbol	Description
bar	bar
mbar	millibar
psi	pounds/sq. inch
Pa	Pascal
hPa	hectoPascal
kPa	kiloPascal
MPa	MegaPascal
mmH_2O	mm water
cmH_2O	cm water
mH_2O	metres water
inH_2O	inches water
ftH_2O	feet water
mmHg	mm mercury
inHg	inches mercury
kgf/cm^2	kg force/sq. cm
atm	atmosphere
Torr	torr

3) State Pressure reference: e.g. gauge

Reference options are:
- gauge
- absolute
- barometric
- sealed gauge
- wet/dry differential
- wet/wet differential

4) State cable lengths and units: Integer values only, e.g. 1m cable, 8 ft. Minimum length 1 m (3 ft) cable (only required on certain electrical connectors). Maximum cable length 100 m (300 ft) for approval options not H0; 200 m (600 ft) for approval option H0.

5) Output options 5, 8 and 9: State voltage output at minimum and maximum pressure: e.g. output –1 to 9 V

Typical order examples:

PTX5012-TB-A2-CA-H0-PA, 0 to 10 bar, gauge, 3 m cable
PMP5028-TD-A3-CC-H0-PE, -15 to 75 psi, gauge, 15ft cable, output voltage -1 to 5 volts
PDCR5071-TB-A1-CB-H0-PB, 0 to 100 bar, sealed gauge

Accessories

Mating connector for MIL-C-26482 (Electrical connector options 6, A, E and F) under part number S_163-009,

Note: Not considered suitable for use in hazardous areas due to light metals content and low ingress protection (IP) rating.

Mechanical Drawings

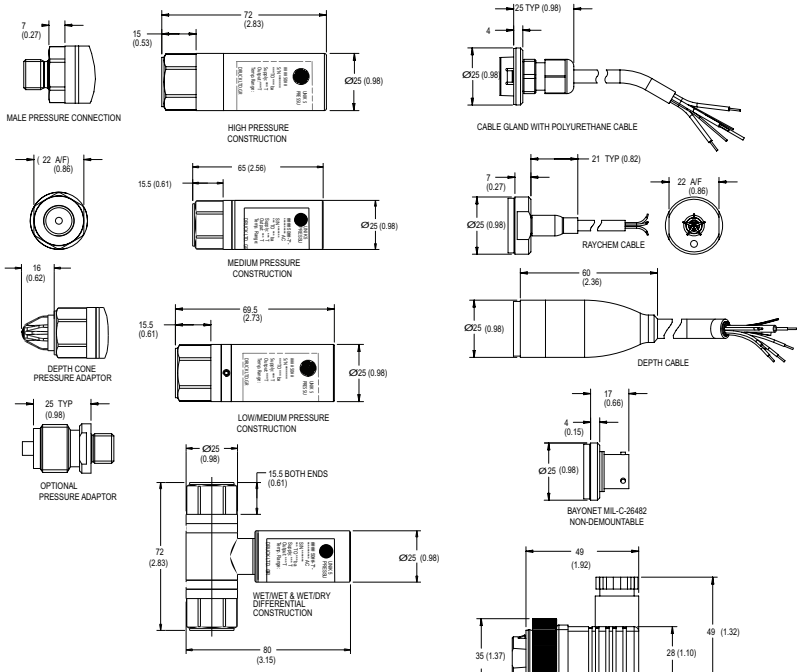

NOTES:

[1] DIMENSIONS SHOWN ARE FOR STANDARD LENGTH PRODUCTS WITH THE FOLLOWING ELECTRICAL OUTPUT OPTIONS:
- mV LINEARISED (PDCR)
- 4 TO 20 mA (PTX)
- STANDARD VOLTAGE OPTIONS (PMP)
- BASIC CONFIGURABLE (PMP)

FOR mV PASSIVE (PDCR) - SUBTRACT 10 mm (0.39 in)
FOR CONFIGURABLE 4-WIRE AND CONFIGURABLE 3-WIRE (PMP) - ADD 15 mm (0.59 in)

[2] REFER TO PAGE 4 FOR LIST OF PRESSURE CONNECTION OPTIONS (ORIENTATION NOT CRITICAL)

[3] ALL DIMENSIONS ARE IN MILLIMETRES (INCHES IN PARENTHESES)

[4] **HIGH PRESSURE IS >70 BAR**
MEDIUM PRESSURE
INDUSTRIAL ACCURACY >1 BAR TO ≤ 50 BAR
LOW/MEDIUM PRESSURE
INDUSTRIAL ACCURACY < 1 BAR, > 50 BAR TO ≤ 70 BAR
IMPROVED/PREMIUM ACCURACY ≤ 70 BAR

www.ge-mcs.com

920-483J

© 2014 General Electric Company. All Rights Reserved. Specifications are subject to change without notice. GE is a registered trademark of General Electric Company. Other company or product names mentioned in this document may be trademarks or registered trademarks of their respective companies, which are not affiliated with GE.

Erlend Røneid

Pressure pulsations at Iveland Power Plant

NTNU
Norwegian University of
Science and Technology